MSc Thesis

Adaptive Feedforward Control for Active Vibration Isolation Systems with Motion Stage and Nonlinear Dynamics

R.Grootkarzijn

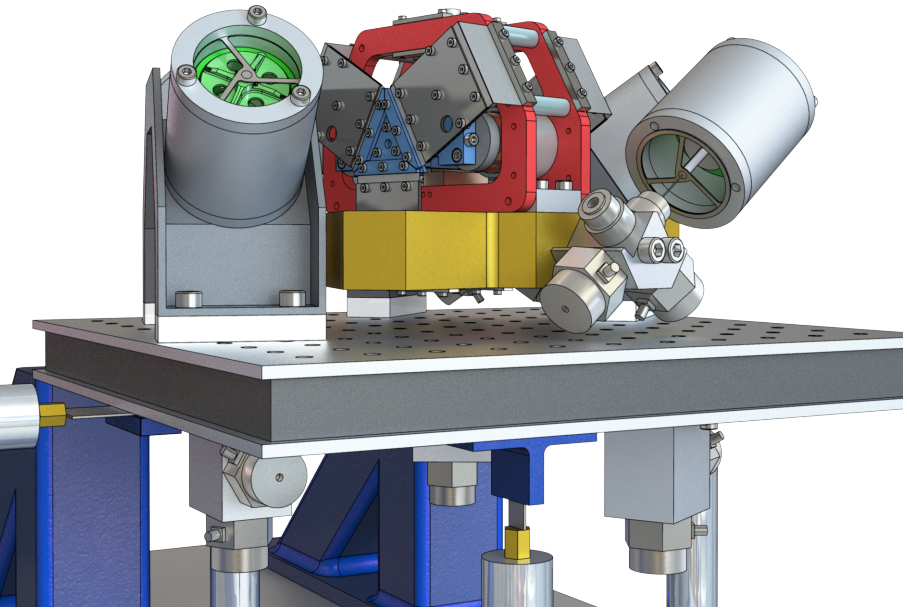

Faculty of Engineering Technology (ET)
Precision Engineering (PE)

Examination committee:

Dr.Ir. W.B.J. Hakvoort

Ir. S.T. Spanjer

Dr.Ir. R.G.K.M. Aarts

Abstract

High precision systems are critical in many scientific and engineering fields. Applications include telescopes, particle colliders, interferometers and lithography machines. Systems like this are subject to disturbances that limit their performance. To attenuate these disturbances, the critical payload is typically suspended to the floor by means of a vibration isolation system. As such, a distinction can be made between direct disturbances, that act directly on the sensitive payload, and indirect disturbances, that enter the system through the suspension. Direct disturbances, for example, could be reaction forces of some process taking place on the critical payload whereas indirect disturbances are usually floor vibrations. The performance of passive vibration isolation systems is characterized by two tradeoffs. The first is expressed in terms of the suspension frequency, where low suspension frequency gives good attenuation of floor vibrations but high sensitivity to direct disturbance forces. For high suspension frequencies this is the other way around. Adding mass attenuates both types of disturbances, however there are some obvious practical limits to the amount of mass that can be added to a system. The second tradeoff is characterized by the relative damping, where increasing the relative damping at the suspension frequency will decrease high frequency indirect disturbance rejection.
Active vibration isolation systems (AVIS) have shown to mitigate the effects of these tradeoffs. Typical active solutions focus on a passive payload. Recently however, this has been extended to a payload with motion stage that introduces additional direct disturbances due to reaction forces. This thesis presents a structured method for deriving the equations of motion of an AVIS with motion stage. The equations of motion are used to construct the disturbance feedforward controllers in a mixed feedback/feedforward control strategy. The performance of feedforward control greatly depends on parameter accuracy. These parameters may be difficult to identify or they can be time-varying, for example due to temperature changes. Therefore, an adaptive algorithm in the form of a filtered-error Kalman approach is proposed and implemented. The control strategy is tested in a simulation environment and implemented on an experimental setup. Substantial performance improvement was observed with respect to the passive and feedback controlled system, especially on axes where disturbances due to motion stage reaction forces were most prominent. Results include a reduction of 91.1% of the power spectral density of the payload acceleration (x-axis) at the fundamental frequency of the motion stage with respect to passive system. At the 3rd harmonic an improvement up to 99.99% was observed. The tracking error of the motion stage reduced with 90% to approximately 300 nm compared to the passive system.

Contents

Introduction

This chapter explains the tradeoffs that exist within passive vibration isolation systems. A discussion on how active vibration isolation systems attempt to mitigate the effects of these tradeoffs is provided. Finally, an overview on the current state of the art is given along with the research challenges and contributions of this thesis.

2.1 Background

High precision systems are critical in many scientific and engineering fields. Typical applications include telescopes, particle colliders, interferometers and lithography machines [1]. Systems like this are subject to various disturbances, for example floor vibrations, that limit their performance. In general, a sensitive payload is connected to the floor via a suspension system [2], [3], as illustrated in figure 2.1

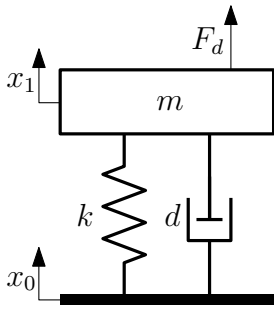

Figure 2.1: Passive vibration isolation system where x_0 and x_1 represent the position of the floor and sensitive payload respectively.

Usually the disturbances a categorized as either direct or indirect. As the name suggests, direct disturbances act directly on the sensitive payload whereas indirect disturbances enter the system through the suspension. Passive solutions to attenuate indirect (floor) disturbances introduce tradeoffs in terms of transmissibility (2.1) and compliance (2.2).

$$T(s) = \frac{\ddot{x}_1(s)}{\ddot{x}_0(s)} = \frac{ds + k}{ms^2 + ds + k} \tag{2.1}$$

$$C(s) = \frac{x_1(s)}{F_d(s)} = \frac{1}{ms^2 + ds + k} \tag{2.2}$$

If the suspension frequency is defined as ω_n then using $\frac{k}{m} = \omega_n$ and $\frac{d}{m} = 2\zeta\omega_n$, equations 2.1 and 2.2 can be rewritten as

$$T(s) = \frac{2\zeta\omega_n s + \omega_n^2}{s^2 + 2\zeta\omega_n s + \omega_n^2} \tag{2.3}$$

$$C(s) = \frac{\omega_n^2}{s^2 + 2\zeta\omega_n s + \omega_n^2}\frac{1}{k}. \tag{2.4}$$

From 2.3 and 2.4 the first tradeoff can now be derived, which is characterized by the suspension frequency. Lowering the suspension frequency will improve indirect disturbance rejection at higher frequencies but will deteriorate direct disturbance rejection at lower frequencies. This is illustrated in figure 2.2.

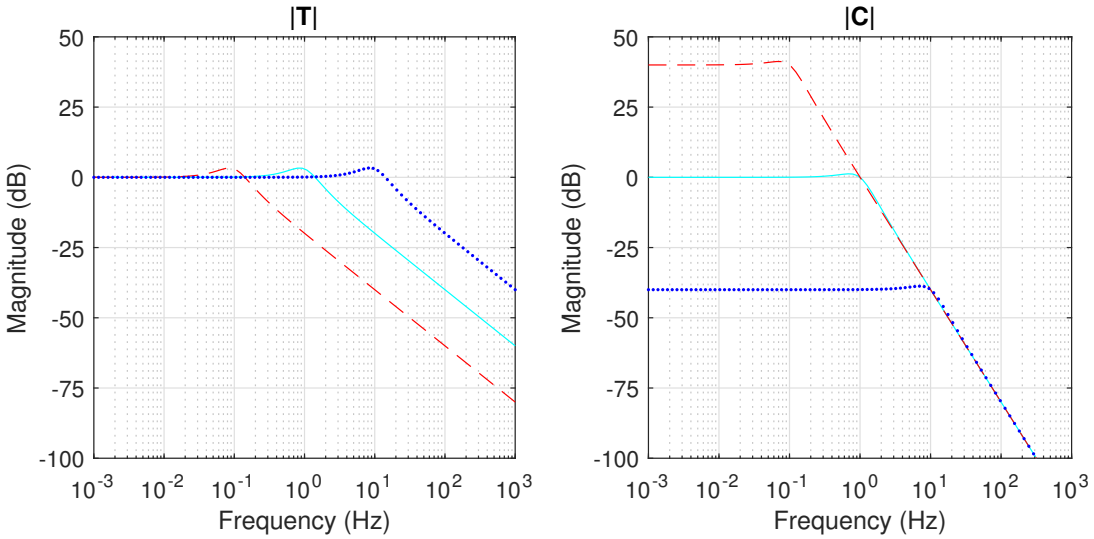

Figure 2.2: Transmissibility and compliance for suspension frequencies of 0.1 (dashed), 1 (solid) and 10 (dotted) Hz

The second tradeoff is characterized by the relative damping. Increasing the relative damping at the suspension frequency will decrease high frequency indirect disturbance rejection, as shown in figure 2.3.

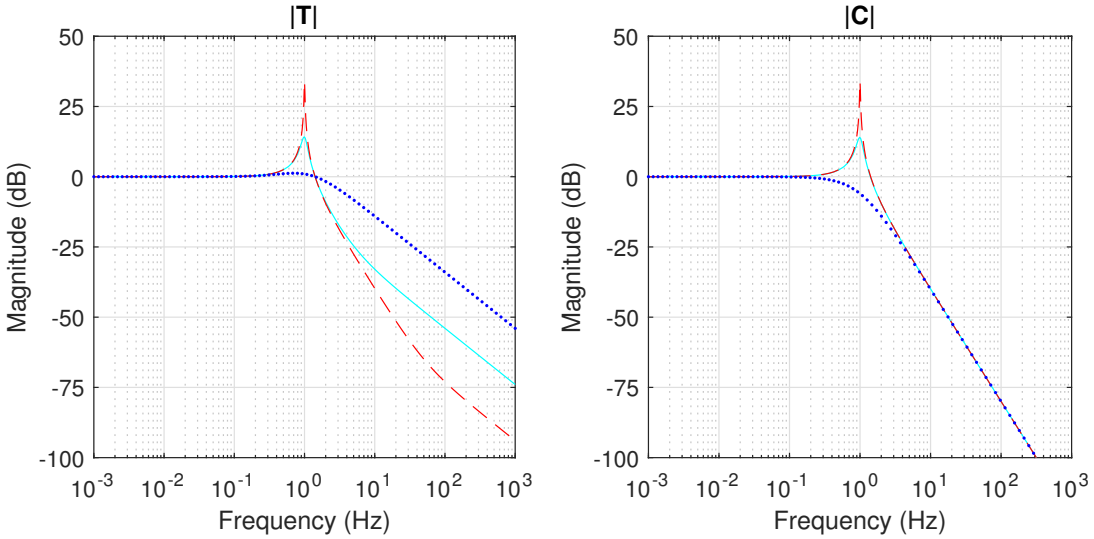

Figure 2.3: Transmissibility and compliance for a relative damping of 0.01 (dashed), 0.1 (solid) and 1 (dotted)

In more general terms, passive systems always require some application specific balance between direct and indirect disturbance rejection which is determined by choice of suspension frequency and relative damping. This poses some difficult design choices when active elements are present on the critical payload in which case direct disturbances, such as reaction forces, can become a dominant factor. Typically, the balance would shift towards a hard-mount setup [4], which makes the process more susceptible to indirect disturbances. Active vibration isolation has shown to mitigate the effects of presented tradeoffs [5].

2.2 Active vibration isolation

Active disturbance attenuation can, to some extent, be achieved trough classical feedback control. Typical solutions include Skyhook damping, virtual balance mass and force feedback [2]–[4]. In addition, disturbance-observer-based methods provide a more modular approach which can be particularly useful when reference tracking is involved and when specific types of disturbances are considered [6]. Feedback control, however, also comes with several challenges imposed by the physical properties of the system and sensor noise. In closed loop systems stability has to be considered, usually by means of the Nyquist criterion. Additionally, there is Bode's sensitive integral such that disturbance attenuation in a certain frequency band will always lead to disturbance amplification in another, commonly known as the waterbed effect. Performance gain will therefore always be limited.

Disturbance feedforward control does not introduce the aforementioned stability issues. It requires measurement of some variable that correlates to the primary disturbance. The general idea is that a secondary disturbance with opposite phase is produced to cancel the primary disturbance [2]. The performance gain of feedforward control relies on several factors such as model accuracy and the correlation between the measured variable and the disturbance [7]. Even though some limitations of passive systems can be addressed, active control comes with its own tradeoffs and limitations.

A mixed control strategy where feedback is combined with disturbance feedforward control appears to be promising method [3], [8]. Here, floor vibrations (indirect disturbances) are measured and used to create a secondary disturbance of opposite phase to cancel payload vibrations. An advantage of using a floor vibration measurement (disturbance feedforward) is that it generally gives a better signal-to-noise ratio then using critical payload measurement (feedback) where the disturbances may already be partly filtered by the suspension system [9]. Measuring and discretization, however, will always introduce delays. Therefore, a perfect feedforward controller that is also practically implementable (e.g. causal) does not exist. An alternative solution is found in solving the H_2 optimal control problem which results in the Wiener filter [7]. Combined with a model based approach a highly efficient formulation of the feedforward controller is obtained [10]. Since the reference signal is measured and not generated, disturbance feedforward control is limited in performance by the waterbed effect, similar to Bode's sensitivity integral for feedback systems [9].

As mentioned, model accuracy of one the key aspects in performance gain of feedforward control as the controller coefficients are based on some system model. In practice, model errors may arise because system parameters can be hard to identify [11] or vary in time, for example due to changes in temperature. Model accuracy may be improved through adaptation algorithms. Least mean squares (LMS) based variants are such as FxLMS, FuLMS and FeLMS are widely used. The coefficients are adapted through an LMS algorithm using the measured residual disturbance. With FxLMS, the regressor is constructed by filtering the reference signal by an estimated model of the secondary path. FuLMS can be interpreted as an IIR extension to FxLMS where the regressor is extended with controller output 'u' to account for any feedback dynamics from 'u' to the reference. FeLMS differs from FxLMS by the fact that the error, or residual disturbance, is filtered instead of the reference. For MIMO systems where the number of inputs exceeds the number of outputs the latter is usually more efficient. LMS based algorithms are attractive for their low computational loads, however in their original definition convergence speed is typically low. Methods such as preconditioning may reduce this effect. Similar variants can be found in recursive least squares (RLS) algorithms, which minimize the mean square error instead of the instantaneous error that is minimized by LMS algorithms. An FeRLS approach appears to be superior to FeLMS in terms of steady-state parameter variance, convergence uniformity and speed [12].

Up to this point only active vibration isolation systems with a passive payload have been considered. However, payload with active elements comprise an important class of systems [13]. Recently, promising results have been obtained for an AVIS with motion stage and compliant frame mode [8]. Here, the disturbance feedforward controller is extended with information from the motion stage, acting as a virtual balance mass. The provided framework will serve as basis for this thesis.

2.3 Objectives and contributions

With the addition of a motion stage and complient frame mode, additional disturbance forces are introduced into the system. As such, a linear approach in construction of the equations of motion may not be sufficiently accurate for model based feedforward control. It is therefore desired that the non-linear equations of motion are derived for an AVIS with motion stage and complient frame mode. As such, a systematic method for determining the equations of motion of the system shall be provided and implemented. The equations will serve as a basis for model based controller design.

Parameter adaptation has shown promising results in combination with disturbance feedforward control [8], [10], [12]. Several LMS and RLS algorithms exist, each with their own advantages and disadvantages. Recent work on an AVIS with motion stage and complient frame mode [8] proposed a combination of a filtered-error LMS algorithm for the critical payload parameters along with a Kalman filter for the motion stage parameters. However, a filtered-error RLS algorithm has shown to be practically implementable while holding some important advantages over LMS algorithms [12]. In this thesis a filtered-error Kalman algorithm, of which the filtered-error RLS algorithm is a special case, is proposed and implemented for both the critical payload en motion stage parameters. A wide variety of Kalman filters have been researched and used extensively which makes that resources for common issues [14] and specific usecases are plentiful. Inspired by [12], the filter can be implemented in a computational highly efficient manner with only some

mild assumptions.

Testing and debugging control algorithms can be a difficult task as they get increasingly more complex. Desired parameters may not be readily available for measurement, hard to identify or there can be (unknown) disturbances. Additionally, it may not be possible to analyze some parts of a system individually but only as part of a whole system. A simulation model provides may help to overcome these issues and is a good starting point for any control system design. Therefore, a three-dimensional model of the proposed framework [8] shall be implemented in a simulation environment to test the developed control algorithm. Additionally, results of the simulation shall be validated experimentally on a benchmark system.

System dynamics and control strategy

First a modeling scheme for an AVIS is presented. Then a systemic method for deriving equations of motions is discussed and applied to the model. Subsequently, a mixed feedback/feedforward control scheme is designed in which the feedforward controllers are generated from the equations of motion. Finally, a novel adaption law is proposed to update the feedforward parameters.

3.1 System description

An ideal physical model (2D) of an active vibration isolation system with motion stage and compliant frame mode is provided in figure 3.1 [8].

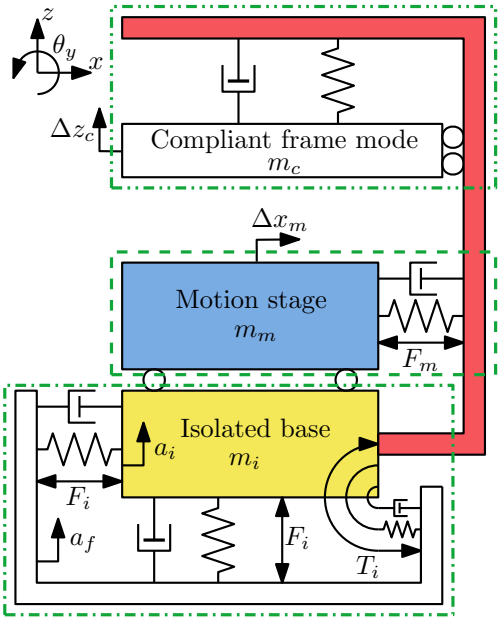

Figure 3.1: Ideal physical model of an AVIS with motion stage and compliant frame mode, where the AVIS comprises the floor, suspension, isolated base and the respective actuators.

A total of four bodies can be distinguished, being the floor (f), isolated base (i), motion stage and compliant frame mode (c). From here on, related parameters will be denoted with the subscripts $\{f, i, m, c\}$ respectively. The isolated base is suspended to the floor by means of springs and dampers. It is host to some critical process that requires high accuracy such as measurement or positioning actions. Thus, it may represent some platform or machine frame whereas the motion stage represents the critical process. The motion stage is suspended to the frame of the isolated base. Actuation of the motion stage generates reaction or direct disturbance forces on the isolated base. Finally, there is the frame deformation as a result of finite frame stiffness, which is represented by the compliant frame mode.
Note that Δx_m and Δz_c are displacements of the motion stage and compliant frame mode with respect to their initial positions and expressed in the coordinate frame of the isolated base. Figure 3.1 is depicted as a 2D planar schematic, but it is easily interpreted in three dimensions. The only DOF of the motion stage is the x-direction in the local coordinate frame of the isolated base. In all other local directions the connection between motion stage and isolated base is considered rigid. In similar fashion, the only DOF of the compliant frame mode is the z-direction in the local coordinate frame of the isolated base and in all other directions their connection is considered rigid. The floor is regarded rheonomic and can be seen as a disturbance input [5].

In the light of a 3D interpretation, all six degrees of freedom of the isolated base ($\boldsymbol{x}_i, \boldsymbol{y}_i, \boldsymbol{z}_i, \boldsymbol{\theta}_{i,x}, \boldsymbol{\theta}_{i,y}, \boldsymbol{\theta}_{i,z}$) are actuated, allowing disturbance attenuation in every direction.

3.2 Constrained equations of motion in augmented form

In this section the equations of motion of the AVIS will be derived. They are used to identify relevant forces and serve as a basis for controller design and implementation. The approach of constrained equations of motion in augmented form [15] is adopted. The main contribution to this application is that it provides a structured formulation in terms of the kinematic constraints and system parameters, as shown in 3.4.

The first step is to define the generalized coordinate vector $\boldsymbol{q}$ that describes the origins of the local coordinate frames of each body, expressed in some inertial frame of reference. These coordinate frames are typically located in the center of mass of each body. When elasticity of bodies is considered, q may contain more coordinates per body, however that is not the case here. The generalized coordinate vector is, however, extended with the two local coordinates Δx_m and Δz_c. This will greatly simplify the process of constructing the equations. The coordinates related to each body are denoted by $\boldsymbol{x}_* \in \mathbb{R}^{6\times 1}$ with $* = \{f, i, m, c\}$, such that the generalized coordinate vector is defined by

$$\boldsymbol{q} = \begin{bmatrix}\boldsymbol{x}_f & \boldsymbol{x}_i & \boldsymbol{x}_m & \boldsymbol{x}_c & \Delta x_m & \Delta z_c\end{bmatrix}^T \in \mathbb{R}^{26\times 1}. \tag{3.1}$$

The inertial frame of reference (O) is located at the 'radial center' of the AVIS such that, in steady state, the center of masses are aligned along its z-axis as illustrated in figure 3.2a. The offsets of the floor, isolated base, motion stage and compliant frame mode are defined by h_f, h_i, h_m and h_c respectively. The floor frame is chosen such that it coincides with the frame of the isolated base so $h_f = h_i$, as illustrated in figure 3.2b.

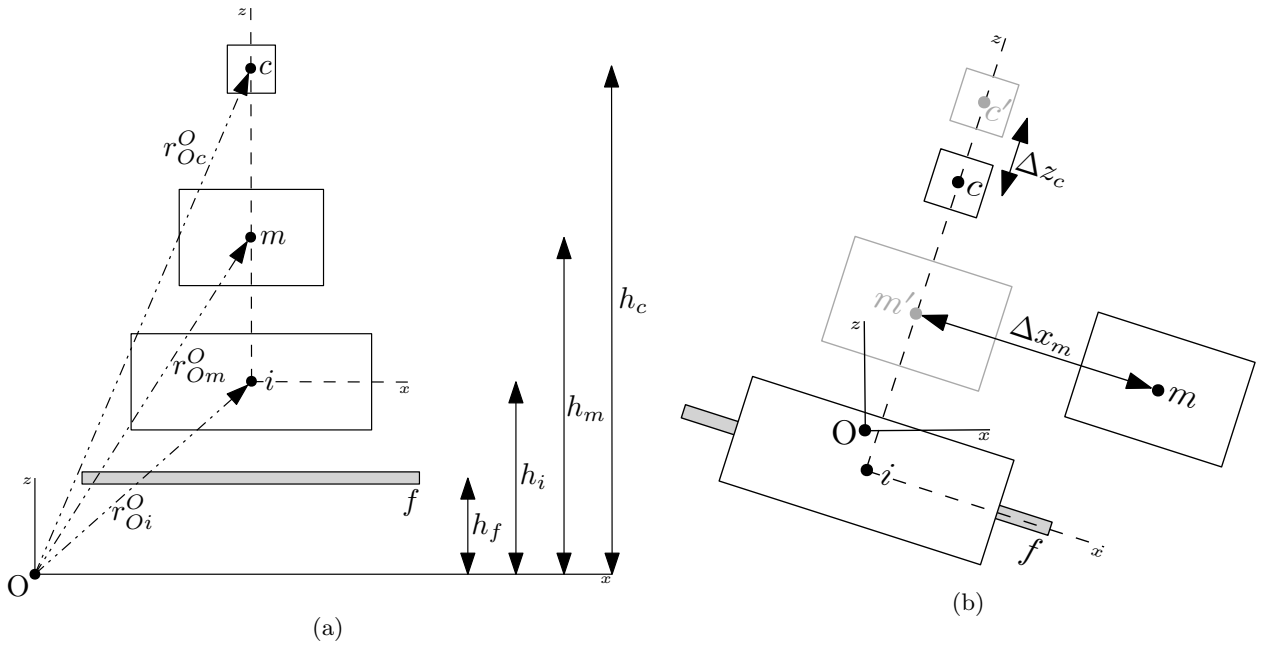

Figure 3.2: Schematic of the floor, isolated base, motion stage and compliant frame mode in relation to frame O.

For vectors the notation r^c_{ab} is used, meaning the vector from a to b expressed in frame c. In the same light, θ^c_{ab} refers to the angle between a and b expressed in frame c. Then based on figure 3.2, the constraint equations can be formulated as

$$\boldsymbol{C}(\boldsymbol{q}) = \begin{bmatrix} \boldsymbol{r}^i_{im} - \begin{bmatrix}\Delta x_m \\ 0 \\ h_m - h_i\end{bmatrix} \\ \boldsymbol{\theta}^i_{im} \\ \boldsymbol{r}^i_{ic} - \begin{bmatrix}0 \\ 0 \\ \Delta z_c + h_c - h_i\end{bmatrix} \\ \boldsymbol{\theta}^i_{ic} \end{bmatrix} = 0, \tag{3.2}$$

where $\{\boldsymbol{r}^i_{im},\, \boldsymbol{\theta}^i_{im},\, \boldsymbol{r}^i_{ic},\, \boldsymbol{\theta}^i_{ic}\} \in \mathbb{R}^{3\times 1}$. Thus, Δx_m is defined as the relative x position of the motion stage expressed in the frame of the isolated base. As such, Δz_c is defined as the relative z position of the compliant frame mode expressed in the frame of the isolated base. The orientation of the motion stage and compliant frame mode are always equal to the orientation of the isolated base. Rewriting in terms of vectors expressed in the inertial frame gives

$$\boldsymbol{C}(\boldsymbol{q}) = \begin{bmatrix} \boldsymbol{R}^O_{Oi}(\boldsymbol{r}^O_{Om} - \boldsymbol{r}^O_{Oi}) - \begin{bmatrix} \Delta x_m \\ 0 \\ h_m - h_i \end{bmatrix} \\ \boldsymbol{\theta}^O_{Om} - \boldsymbol{\theta}^O_{Oi} \\ \boldsymbol{R}^O_{Oi}(\boldsymbol{r}^O_{Oc} - \boldsymbol{r}^O_{Oi}) - \begin{bmatrix} \Delta z_c \\ 0 \\ h_c - h_i \end{bmatrix} \\ \boldsymbol{\theta}^O_{Oc} - \boldsymbol{\theta}^O_{Oi} \end{bmatrix} = 0, \tag{3.3}$$

where $\boldsymbol{R}^O_{Oi} \in \mathbb{R}^{3\times 3}$, $\{\boldsymbol{r}^O_{Om},\, \boldsymbol{r}^O_{Oi},\, \boldsymbol{r}^O_{Oc},\, \boldsymbol{\theta}^O_{Om},\, \boldsymbol{\theta}^O_{Oi},\, \boldsymbol{\theta}^O_{Oc}\} \in \mathbb{R}^{3\times 1}$. The next step is to apply the equations of motion in augmented form given by

$$\begin{bmatrix} \boldsymbol{M} & \boldsymbol{\Phi}_q^T \\ \boldsymbol{\Phi}_q & \boldsymbol{0} \end{bmatrix} \begin{bmatrix} \ddot{\boldsymbol{q}} \\ \boldsymbol{\lambda} \end{bmatrix} = \begin{bmatrix} \boldsymbol{Q}_A - \boldsymbol{D}\dot{\boldsymbol{q}} - \boldsymbol{K}\boldsymbol{q} \\ \boldsymbol{\gamma} \end{bmatrix} \tag{3.4}$$

Here, $\boldsymbol{Q}_A$ contains the applied forces such as gravity and actuator forces. $\boldsymbol{M}$, $\boldsymbol{D}$ and $\boldsymbol{K}$ contain the mass, damping and stiffness properties of the respective elements. The constraint forces are included in Lagrange multiplier form as $\boldsymbol{\Phi}_q^T\boldsymbol{\lambda}$, where $\boldsymbol{\Phi}_q^T$ is the Jacobian of the constraint equations found in 3.3 with respect to the generalized coordinate vector $\boldsymbol{q}$. This vector can be partitioned in dependent and independent coordinates where, by choice,

$$\begin{aligned} \boldsymbol{q}^d &= \begin{bmatrix} \boldsymbol{x}_m\ \boldsymbol{\theta}_m\ \boldsymbol{x}_c\ \theta_c \end{bmatrix}^T \in \mathbb{R}^{12\times 1} \\ \boldsymbol{q}^i &= \begin{bmatrix} \boldsymbol{x}_f\ \boldsymbol{\theta}_f\ \boldsymbol{x}_i\ \boldsymbol{\theta}_i\ \Delta x_m\ \Delta z_c \end{bmatrix}^T \in \mathbb{R}^{14\times 1}. \end{aligned} \tag{3.5}$$

Applying this partitioning to the equations of motions gives

$$\begin{bmatrix} \boldsymbol{M}^{dd} & \boldsymbol{M}^{di} & \boldsymbol{\Phi}^T_{\boldsymbol{q}^d} \\ \boldsymbol{M}^{id} & \boldsymbol{M}^{ii} & \boldsymbol{\Phi}^T_{\boldsymbol{q}^i} \\ \boldsymbol{\Phi}^T_{\boldsymbol{q}^d} & \boldsymbol{\Phi}^T_{\boldsymbol{q}^i} & \boldsymbol{0} \end{bmatrix} \begin{bmatrix} \ddot{\boldsymbol{q}}^d \\ \ddot{\boldsymbol{q}}^i \\ \boldsymbol{\lambda} \end{bmatrix} = \begin{bmatrix} \boldsymbol{Q}^d_A \\ \boldsymbol{Q}^i_A \\ \boldsymbol{\gamma} \end{bmatrix} - \begin{bmatrix} \boldsymbol{D}^{dd} & \boldsymbol{D}^{di} \\ \boldsymbol{D}^{id} & \boldsymbol{D}^{ii} \\ \boldsymbol{0} & \boldsymbol{0} \end{bmatrix} \begin{bmatrix} \dot{\boldsymbol{q}}^d \\ \dot{\boldsymbol{q}}^i \\ \boldsymbol{0} \end{bmatrix} - \begin{bmatrix} \boldsymbol{K}^{dd} & \boldsymbol{K}^{di} \\ \boldsymbol{K}^{id} & \boldsymbol{K}^{ii} \\ \boldsymbol{0} & \boldsymbol{0} \end{bmatrix} \begin{bmatrix} \boldsymbol{q}^d \\ \boldsymbol{q}^i \\ \boldsymbol{0} \end{bmatrix}. \tag{3.6}$$

Then because of the additional coordinates Δx_m and Δz_c in combination with 3.5, the subsets of the stiffness and damping matrices related to the dependent coordinates are zero, thus the following equations are obtained.

$$\begin{bmatrix} \boldsymbol{M}^{dd} & \boldsymbol{M}^{di} & \boldsymbol{\Phi}^T_{\boldsymbol{q}^d} \\ \boldsymbol{M}^{id} & \boldsymbol{M}^{ii} & \boldsymbol{\Phi}^T_{\boldsymbol{q}^i} \\ \boldsymbol{\Phi}^T_{\boldsymbol{q}^d} & \Phi^T_{\boldsymbol{q}^i} & 0 \end{bmatrix} \begin{bmatrix} \ddot{\boldsymbol{q}}^d \\ \ddot{\boldsymbol{q}}^i \\ \boldsymbol{\lambda} \end{bmatrix} = \begin{bmatrix} \boldsymbol{Q}^d_A \\ \boldsymbol{Q}^i_A - \boldsymbol{D}^{ii}\dot{\boldsymbol{q}}^i - \boldsymbol{K}^{ii}\boldsymbol{q}^i \\ \boldsymbol{\gamma}. \end{bmatrix} \tag{3.7}$$

This partitioning allows for rewriting all equations in terms of the independent coordinates. The complete derivation, without stiffness and damping matrices, can be found in [15].

$$\begin{aligned} \left[\boldsymbol{M}^{ii} - \boldsymbol{M}^{id}\boldsymbol{\Phi}^{-1}_{\boldsymbol{q}^d}\boldsymbol{\Phi}_{\boldsymbol{q}^i} - \boldsymbol{\Phi}^T_{\boldsymbol{q}^i}\boldsymbol{\Phi}^{-T}_{\boldsymbol{q}^d}\left[\boldsymbol{M}^{di} - \boldsymbol{M}^{dd}\boldsymbol{\Phi}^{-1}_{\boldsymbol{q}^d}\boldsymbol{\Phi}_{\boldsymbol{q}^i}\right]\right]\ddot{\boldsymbol{q}}^i \\ = \boldsymbol{Q}^i_A - \boldsymbol{M}^{id}\boldsymbol{\Phi}^{-1}_{\boldsymbol{q}^d}\boldsymbol{\gamma} - \boldsymbol{\Phi}^T_{\boldsymbol{q}^i}\boldsymbol{\Phi}^{-T}_{\boldsymbol{q}^d}\left[\boldsymbol{Q}^d_A - \boldsymbol{M}^{dd}\boldsymbol{\Phi}^{-1}_{\boldsymbol{q}^d}\boldsymbol{\gamma}\right] - \boldsymbol{D}^{ii}\dot{\boldsymbol{q}}^i - \boldsymbol{K}^{ii}\boldsymbol{q}^i \end{aligned} \tag{3.8}$$

This can be written in compact form, resulting in the reduced equations of motion

$$\hat{\boldsymbol{M}}\ddot{\boldsymbol{q}}^i = \hat{\boldsymbol{Q}} - \hat{\boldsymbol{D}}\dot{\boldsymbol{q}}^i - \hat{\boldsymbol{K}}\boldsymbol{q}^i \tag{3.9}$$

where

$$\begin{aligned} \hat{\boldsymbol{M}} &= \left[\boldsymbol{M}^{ii} - \boldsymbol{M}^{id}\boldsymbol{\Phi}^{-1}_{\boldsymbol{q}^d}\boldsymbol{\Phi}_{\boldsymbol{q}^i} - \boldsymbol{\Phi}^T_{\boldsymbol{q}^i}\boldsymbol{\Phi}^{-T}_{\boldsymbol{q}^d}\left[\boldsymbol{M}^{di} - \boldsymbol{M}^{dd}\boldsymbol{\Phi}^{-1}_{\boldsymbol{q}^d}\boldsymbol{\Phi}_{\boldsymbol{q}^i}\right]\right] \\ \hat{\boldsymbol{D}} &= \boldsymbol{D}^{ii} \\ \hat{\boldsymbol{K}} &= \boldsymbol{K}^{ii} \\ \hat{\boldsymbol{Q}} &= \boldsymbol{Q}^i_A - \boldsymbol{M}^{id}\boldsymbol{\Phi}^{-1}_{\boldsymbol{q}^d}\boldsymbol{\gamma} - \boldsymbol{\Phi}^T_{\boldsymbol{q}^i}\boldsymbol{\Phi}^{-T}_{\boldsymbol{q}^d}\left[\boldsymbol{Q}^d_A - \boldsymbol{M}^{dd}\boldsymbol{\Phi}^{-1}_{\boldsymbol{q}^d}\boldsymbol{\gamma}.\right] \end{aligned} \tag{3.10}$$

Note that some subsections of the Jacobian and Hessian of the constraint equations may require q^d or $\dot{q}^d$. Then q^d can be found by setting $\Phi_{q^d} = 0$ and solving for $\boldsymbol{q}^d$. This allows $\boldsymbol{q}^d$ to be written in terms of $\boldsymbol{q}^i$. Then $\dot{\boldsymbol{q}}^d = -\boldsymbol{\Phi}_{\boldsymbol{q}^d}^{-1}\boldsymbol{\Phi}_{tt}$ and $\boldsymbol{\gamma} = -\left[\boldsymbol{\Phi}_q\dot{\boldsymbol{q}}\right]_q\dot{\boldsymbol{q}} - 2\boldsymbol{\Phi}_{qt}\dot{\boldsymbol{q}} - \boldsymbol{\Phi}_{tt}$.

For kinematically solvable systems this embedded formulation directly gives a minimal set of equations in terms of the independent coordinates. The problem of obtaining the equations of motion has now mainly been reduced to obtaining the kinematic constraint equations, which is considerably more easy for the system discussed in this thesis. Since the equations of motion contain the actuator forces, they can be used to determine the required actuator forces to cancel all disturbance forces included in the model.

3.3 Controller design

The main objectives of the active vibration isolation system is to ensure proper reference tracking of the motion stage while minimizing internal frame deformation [8]. As such, the following mixed feedback/feedforward control scheme [8] is adopted to attenuate direct and indirect disturbances.

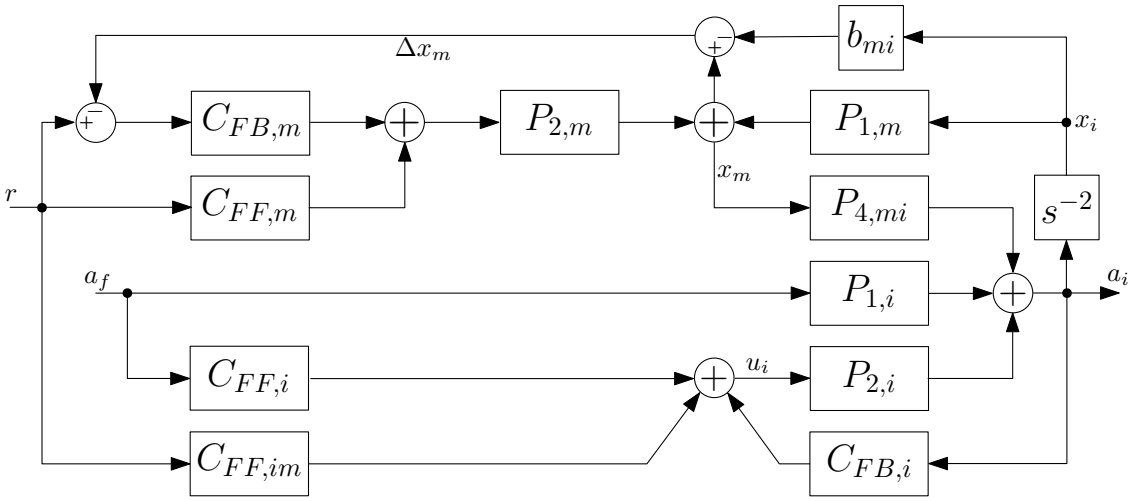

Figure 3.3: Control scheme AVIS

Here $\boldsymbol{P}_{1,i}$ is the primary path where floor vibrations enter the isolated base. $\boldsymbol{P}_{2,i}$ is the secondary path through which actuator forces act on the isolated base. In similar fashion, $P_{1,m}$ is the primary path where isolated base vibrations affect the motion stage and $P_{2,m}$ the secondary path through which the motion stage is actuated. $\boldsymbol{P}_{4,mi}$ models the forces of the motion stage on the isolated base.

Isolated base

For the isolated base we can distinguish three controllers. A feedback controller for direct disturbances and unmodelled dynamics, a feedforward controller to cancel floor disturbances and another feedforward controller to cancel motion stage induced disturbances. For the feedforward controllers a reverse approach is taken. The actuator forces are determined under the assumption of perfect disturbance attenuation. That is, the equations of motion are solved for the actuator forces and the position of the isolated base is assumed zero. The forces for each actuator are then described by

$$\begin{aligned}
F_{i,x} &= -d_{f,x}\dot{x}_f - k_{f,x}x_f + m_m\Delta\ddot{x}_m \\
F_{i,y} &= -d_{f,y}\dot{y}_f - k_{f,y}y_f \\
F_{i,z} &= -d_{f,z}\dot{z}_f - k_{f,z}z_f + (m_i + m_m + m_c)g + m_c\Delta\ddot{z}_c \\
T_{i,x} &= -d_{f,\theta_x}\dot{\theta}_{x,f} - k_{f,\theta_x}\theta_{f,x} \\
T_{i,y} &= -d_{f,\theta_y}\dot{\theta}_{y,f} - k_{f,\theta_y}\theta_{f,y} + m_m g\Delta x_m - m_m\Delta\ddot{x}_m(h_m - h_i) \\
T_{i,z} &= -d_{f,\theta_z}\dot{\theta}_{z,f} - k_{f,\theta_z}\theta_{f,z}
\end{aligned} \tag{3.11}$$

For some axes the required actuator forces depend on both floor and motion stage related variables, confirming the control scheme of 3.3. Δz_c is not actuated and in general not measured, merely a variable which is subject to indirect minimization by cancelling all other disturbances acting on the system. It will therefore not be used in cancellation of disturbance forces. The gravitational term in z-direction is not

considered, as it is not related to any independent coordinate. In case of proper tracking, $\Delta x_m \approx r$. Since r and all its derivates are determined analytically, they are exactly known at all times and no differentiation is required. As a result the actuator forces are approximated in the frequency domain by the follow relations

$$\begin{aligned}
F_{i,x}(s) &= -(d_{f,x}s - k_{f,x})x_f(s) + m_m r(s)s^2 \\
F_{i,y}(s) &= -(d_{f,y}s - k_{f,y})y_f(s) \\
F_{i,z}(s) &= -(d_{f,z}s - k_{f,z})z_f(s) \\
T_{i,x}(s) &= -(d_{f,\theta_x}s - k_{f,\theta_x})\theta_{f,x}(s) \\
T_{i,y}(s) &= -(d_{f,\theta_y}s - k_{f,\theta_y})\theta_{f,y}(s) + m_m g r(s) - m_m(h_m - h_i)r(s)s^2 \\
T_{i,z}(s) &= -(d_{f,\theta_z}s - k_{f,\theta_z})\theta_{f,z}(s).
\end{aligned} \tag{3.12}$$

These equations do not yet include actuator dynamics. For the isolated base six voltage controlled voice coil motors (VCM's) are used to generate the desired actuation forces. Then actuator dynamics can then be included by substituting each force on the lefthand side of equation 3.12 with $F_{i,*}(s) = k_f(Ls + R)^{-1}V_{i,*}(s)$ [16]. Then solving for $V_{i,*}(s)$ by multiplying each side with the inverse actuator dynamics provides the final equation for calculation of the feedforward voltage.

$$\begin{aligned}
\boldsymbol{V}_{FF,i}(s) = -k_{f,i}^{-1} \big[\boldsymbol{D}_f L_i \quad \boldsymbol{K}_f L_i + \boldsymbol{D}_f R_i \quad \boldsymbol{K}_f R_i \quad \boldsymbol{a}_3 \quad \boldsymbol{a}_2 \quad \boldsymbol{a}_1 \quad \boldsymbol{a}_0 \big] \\
\big[\boldsymbol{x}_f s^2 \quad \boldsymbol{x}_f s \quad \boldsymbol{x}_f \quad r s^3 \quad r s^2 \quad r s \quad r \big]^T
\end{aligned} \tag{3.13}$$

where $\boldsymbol{V}_{FF,i}(s) \in \mathbb{R}^{6\times 1}$, $D_f \in \mathbb{R}^{6\times 6}$, $K_f \in \mathbb{R}^{6\times 6}$, $x_f \in \mathbb{R}^{6\times 1}$ and

$$\begin{aligned}
\boldsymbol{a}_3 &= \big[m_m L_i \quad 0 \quad 0 \quad 0 \quad -m_m L_i(h_m - h_i) \quad 0 \big]^T \\
\boldsymbol{a}_2 &= \big[m_m R_i \quad 0 \quad 0 \quad 0 \quad -m_m R_i(h_m - h_i) \quad 0 \big]^T \\
\boldsymbol{a}_1 &= \big[0 \quad 0 \quad 0 \quad 0 \quad m_m g L_i \quad 0 \big]^T \\
\boldsymbol{a}_0 &= \big[0 \quad 0 \quad 0 \quad 0 \quad m_m g R_i \quad 0 \big]^T
\end{aligned} \tag{3.14}$$

The floor accelerations, $x_f(s)s^2$, are directly measured. They will be denoted as $a_f(s)$. The velocity and position can then be obtained by integration. Pure integrators, however, amplify low frequent noise and have infinite DC gain. Therefore, they are approximated by 'weak integrators' [10] using the following structure.

$$H_{a,n}(s) = \frac{1 - L_{a,n}(s)}{s} \tag{3.15}$$

$$L_{a,n}(s) = \left(\frac{\alpha}{\alpha + s}\right)^n \tag{3.16}$$

Here an n^{th}-order low-pass filter is obtained with cut-off frequency α, which is then chosen such that $H_{a,n}(s)$ approximates a pure integrator within the desired frequency band. Rewriting equation 3.13 with the proposed modifications leads to the following notation that is linear in the parameters and where the two feedforward controllers are combined.

$$\begin{aligned}
\boldsymbol{V}_{FF,i}(s) = -k_{f,i}^{-1} \big[\boldsymbol{D}_f L_i \quad \boldsymbol{K}_f L_i + \boldsymbol{D}_f R_i \quad \boldsymbol{K}_f R_i \quad \boldsymbol{a}_3 \quad \boldsymbol{a}_2 \quad \boldsymbol{a}_1 \quad \boldsymbol{a}_0 \big] \\
\big[\boldsymbol{a}_f \quad H_n \boldsymbol{a}_f \quad H_n^2 \boldsymbol{a}_f \quad r s^3 \quad r s^2 \quad r s \quad r \big]^T
\end{aligned} \tag{3.17}$$

In relation to figure 3.3 this can be interpreted as

$$\boldsymbol{V}_{FF,i}(s) = \big[\boldsymbol{C}_{FF,i} \quad \boldsymbol{C}_{FF,im} \big] \begin{bmatrix} \boldsymbol{a}_f(s) \\ \boldsymbol{r}(s) \end{bmatrix} \tag{3.18}$$

For the feedback controller $C_{FB,i}$ proportional velocity feedback, or Skyhook damping, is chosen. This is implemented by integrating the isolated base acceleration with weak integrators according to the following structure

$$\boldsymbol{C}_{FB,i} = \frac{\omega_i}{1 + \omega_i} k_v \boldsymbol{I_6}. \tag{3.19}$$

The weak integrators have a cutoff frequency of 1 rad/s and the proportional gain k_v is tuned such that relative damping of approximately 0.7 is achieved at the resonance frequency [12].

Motion stage

As a prerequisite for 3.17, accurate reference tracking was assumed. It is therefore crucial to implement a proper controller. Inversion based feedforward control allows for high performance reference tracking in motion systems [17]. This could lead to causality issues for plants with relative degree ≥ 1, but since the reference signal and all its derivates can be determined analytically this is not a problem here [18]. The motion stage is actuated by current controlled VCM's. Therefore, there is no additional pole as was the case for the isolated base. The nominal plant model is then given by

$$P_{nom} = \frac{\frac{1}{m_{eq}}}{s^2 + \frac{d}{m}s + \frac{k}{m}}. \tag{3.20}$$

Then the feedforward controller can be written linear in the parameters as

$$I_{FF,m}(s) = m_{eq}\begin{bmatrix}1 & \frac{d_m}{m_m} & \frac{k_m}{m_m}\end{bmatrix}\begin{bmatrix}rs^2 & rs & r\end{bmatrix}^T \tag{3.21}$$

In order to account for robust stability and to improve disturbance rejection, a feedback controller is added in the form of a PID+ controller [19]. This controller adds some phase lead at the desired crossover frequency and the '+' is for the additional high frequency rolloff. The latter provides some extra robustness against parasitic modes. This controller is designed using the following structure.

$$\begin{aligned}\tau_i &= \frac{\sqrt{\frac{1}{\alpha}}}{\omega_c}\\ \tau_p &= \frac{1}{\sqrt{\frac{1}{\alpha}}\omega_c}\\ k_p &= \frac{m_{eq}\omega_c^2}{\sqrt{\frac{1}{\alpha}}}\\ K(s) &= k_p\frac{(s^2\tau_i^2 + 2\zeta_n\tau_i s + 1)}{s\tau_i(s^2\tau_p^2 + 2\zeta_d\tau_p s + 1)}\end{aligned} \tag{3.22}$$

where $\alpha = 0.1$, $\omega_c = 100$ Hz and $\zeta_{n,d} = \frac{1}{\sqrt{2}}$. The stability margins can then be obtained from figures 3.4 and 3.5.

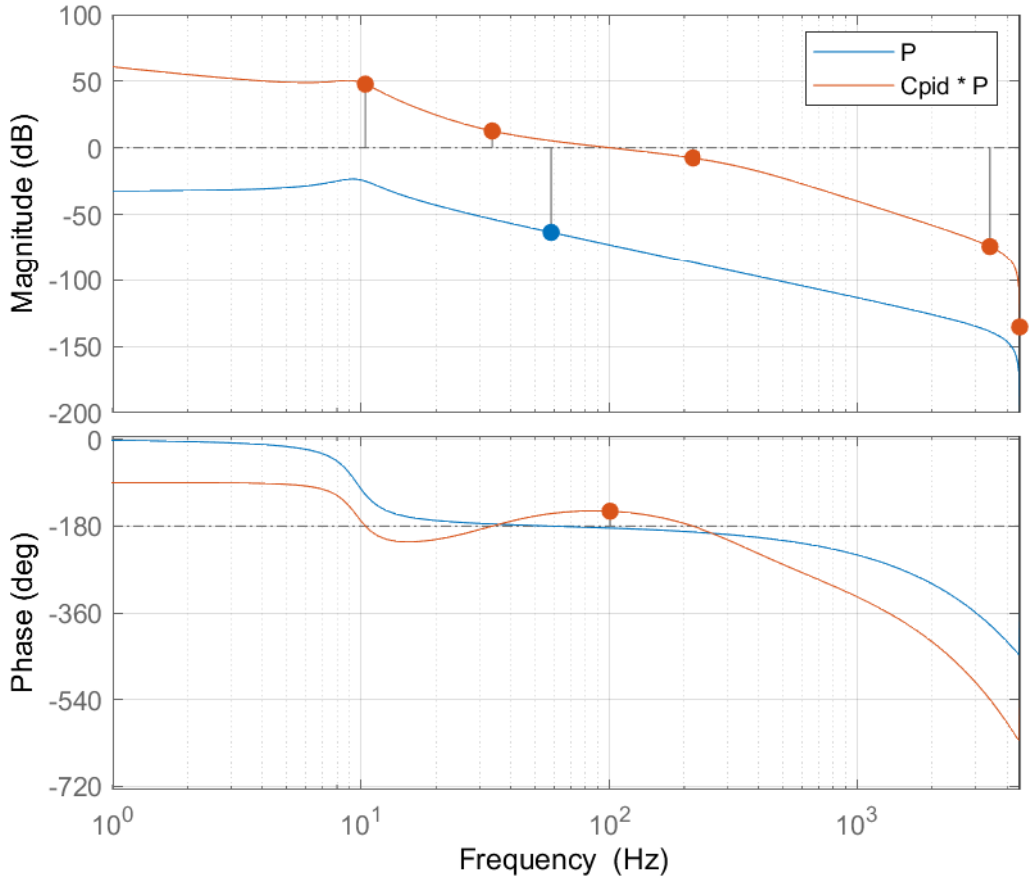

Figure 3.4: Bode plot of nominal plant model of the motion stage P_m and $C_{PID} \cdot P_m$

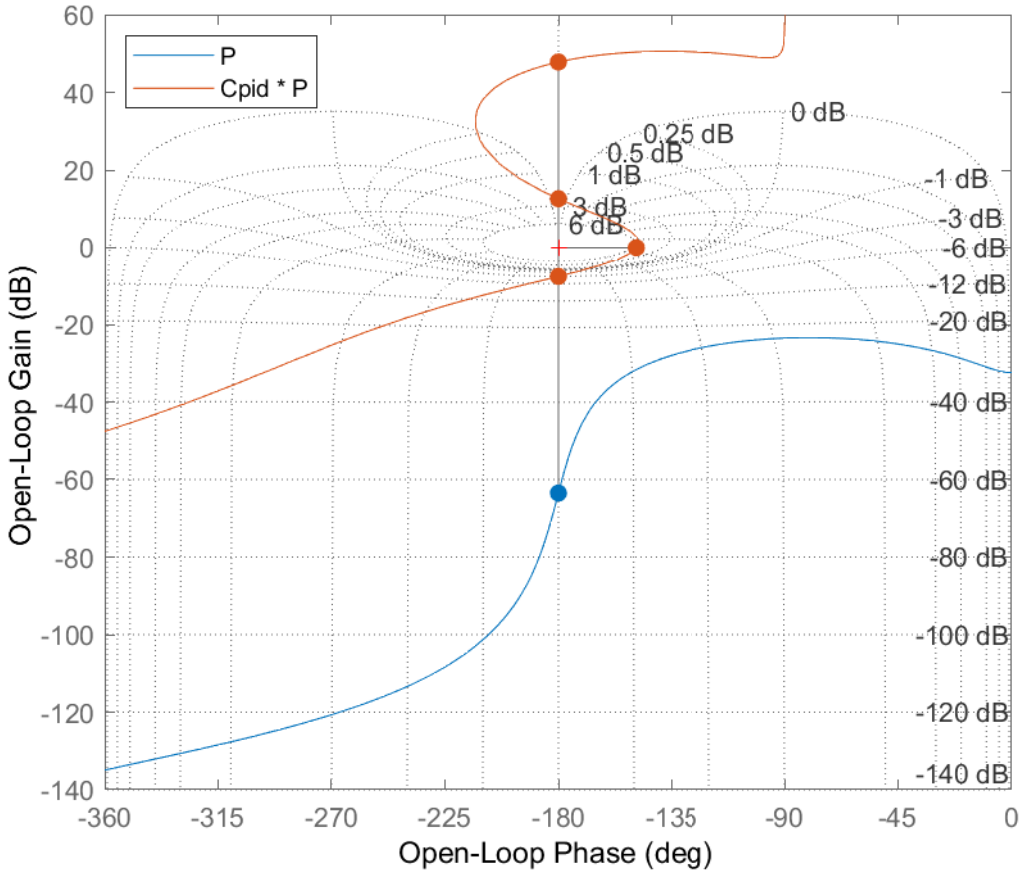

Figure 3.5: Nichols plot of nominal plant model of the motion stage P_m and $C_{PID} \cdot P_m$

The smallest two gain margins are 7.61 dB at 217 Hz and 12.6 dB at 33.7 Hz. Phase margin is 30.9 deg at 101 Hz. Because of the phase lead at the crossover frequency, the bandwidth is a lot larger than would have been possible with for example just proportional feedback. The complex pole accounts for the additional high frequency rolloff for possible parasitic modes, which are not present in the model but may be in practice.

3.4 Control strategy

By linearizing the equations of motion around the initial position, an approximation of the transfer functions in figure 3.3 is obtained. The primary path of the isolated base is the transfer function from floor vibrations a_f to isolated base vibrations a_i. It is denoted by

$$\boldsymbol{P}_{1,i} = \boldsymbol{G}(\boldsymbol{D}_i s + \boldsymbol{K}_i), \tag{3.23}$$

where $\boldsymbol{D}_i$ and $\boldsymbol{K}_i$ contain the damping and spring properties of the isolated base. The secondary path of the isolated base describes the relation between actuator input voltage and acceleration and is given by

$$\boldsymbol{P}_{2,i} = s^2 \boldsymbol{G} \boldsymbol{P}_{a,i}. \tag{3.24}$$

The common factor G is given by

$$\boldsymbol{G} = (\boldsymbol{M}_i s^2 + \boldsymbol{D}_i s + \boldsymbol{K}_i)^{-1}, \tag{3.25}$$

where $\boldsymbol{M}_i$ contains the mass properties of the isolated base. The isolated base actuator dynamics are

$$\boldsymbol{P}_{a,i} = \boldsymbol{K}_{f,i}(L_i s + R_i)^{-1}, \tag{3.26}$$

where $\boldsymbol{K}_{f,i}$ is a diagonal matrix with force constants and L_i and R_i the armature self-inductance and resistance. Then the motion stage primary path describes the relation between isolated base position and motion stage position. It is given by

$$P_{1,m} = g_m(d_m s + k_m), \tag{3.27}$$

where d_m and k_m contain the damping and spring properties of the motion stage. The motion stage secondary path is given by

$$P_{2,m} = g_m k_{f,m} \tag{3.28}$$

where $k_{f,m}$ is the actuator force constant. In similar fashion to the isolated base, there is a common factor g_m which given by

$$g_m = (m_m s^2 + d_m s + k_m)^{-1} \tag{3.29}$$

where m_m contains the mass properties of the motion stage. Looking at figure 3.3 we obtain the following transfer functions. For the motion stage

$$\mathbb{S}_m^{-1} x_m(s) = (P_{1,m} + P_{2,m} C_{FB,m} b_{mi}) s^{-2} a_i(s) + (P_{2,m}(C_{FF,m} + C_{FB,m})) r(s) \tag{3.30}$$

where the motion stage sensitivity is given by

$$\mathbb{S}_m = (I + P_{2,m} C_{FB,m})^{-1}. \tag{3.31}$$

Then for the isolated base the following relation is obtained

$$\mathbb{S}_i^{-1} \boldsymbol{a}_i(s) = (\boldsymbol{P}_{1,i} + \boldsymbol{P}_{2,i} \boldsymbol{C}_{FF,i}) \boldsymbol{a}_f(s) + (\boldsymbol{P}_{2,i} \boldsymbol{C}_{FF,im} + \boldsymbol{P}_{4,mi} \mathbb{S}_m P_{2,m}(C_{FF,m} + C_{FB,m})) r(s) \tag{3.32}$$

where the sensitivity is given by

$$\mathbb{S}_i = (\boldsymbol{I} - \boldsymbol{P}_{2,i} \boldsymbol{C}_{FB,i} - \boldsymbol{P}_{4,mi} \mathbb{S}_m (P_{1,m} + P_{2,m} C_{FB,m} \boldsymbol{b}_{mi}) s^{-2})^{-1} \tag{3.33}$$

Then the required feedforward controllers in terms of these general transfer functions can be derived. The feedforward controller of the motion stage is given by

$$C_{FF,m} = P_{2,m}^{-1}. \tag{3.34}$$

In a similar fashion the optimal feedforward controller for the isolated base is

$$\boldsymbol{C}_{FF,i} = -\boldsymbol{P}_{2,i}^{-1} \boldsymbol{P}_{1,i}. \tag{3.35}$$

Then substituting these controllers in equation 3.32 gives

$$\mathbb{S}_i^{-1} \boldsymbol{a}_i(s) = (\boldsymbol{P}_{2,i} \boldsymbol{C}_{FF,im} + \boldsymbol{P}_{4,mi} \mathbb{S}_m \underbrace{(I + P_{2,m} C_{FB,m})}_{\mathbb{S}_m^{-1}}) r(s) = (\boldsymbol{P}_{2,i} \boldsymbol{C}_{FF,im} + \boldsymbol{P}_{4,mi}) r(s) \tag{3.36}$$

such that the feedforward controller to attenuate disturbances induced by the motion on the isolated base is given by

$$\boldsymbol{C}_{FF,im} = -\boldsymbol{P}_{2,i}^{-1} \boldsymbol{P}_{4,mi}, \tag{3.37}$$

concluding the definition for all feedforward controllers. Note that filling in the transfer functions provided by 3.23 - 3.26 into the feedforward controller definitions of the isolated base, 3.35 and 3.37, will result in the feedforward controller equations derived previously in 3.17.
There are several limitations that must be considered. As stated, accurate reference tracking is critical because of substitution of the motion stage position by the reference signal as controller input. Another limitation arises due to the use of 'weak integrators'. Since the approximation of the pure integrators deteriorates quickly below the chosen α, performance is limited for lower frequencies. Also, the accuracy of the feedforward leans heavily on system parameters. A slight mismatch, for example due to temperature drift or identification accuracy limitations, may decrease controller performance. Figure 3.6 shows the effect of both the 'weak integrators' and parameter mismatch on the transmissibility and reference compliance.

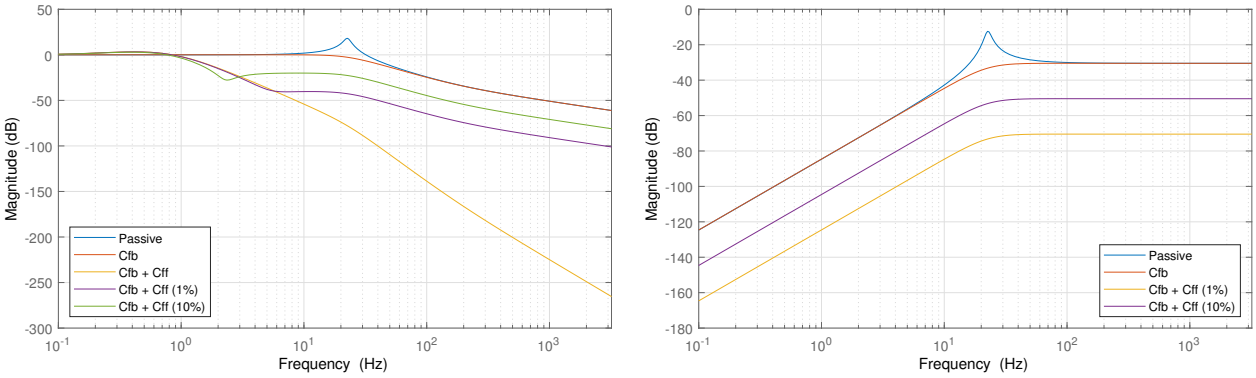

(a) Theoretical transmissibility

(b) Theoretical reference compliance

Figure 3.6: Transmissibility and reference compliance for different controller combinations

Here, 'weak integrators' are used where $\alpha = 1$ Hz. Even with 'perfect' feedforward control, there is very little performance gain with respect to the transmissibility below α. Also, parameters mismatch appears to greatly diminish the performance of both the transmissibility and reference compliance.

3.5 Adaptation

Parameter adaptation is a widely used method to deal with parameter variation and uncertainty. Since all feedforward controllers for both the isolated base and motion stage are linear in the parameters, an adaptation algorithm can be used to update the parameters. In general, the update law follows by minimization of some relevant error. Recent work shows that an FeRLS approach is implementable in real time and can achieve good vibration isolation [12]. The modified filtered-RLS algorithm is shown to be a specific case of the Kalman algorithm where no uncertainty in the secondary path is assumed [7]. In this thesis the Kalman algorithm is applied in combination with the filtered error approach. The proposed exploitation of regression matrix sparsity from [12] is adopted to ensure real time implementation.
Equations 3.38 and 3.39 show the isolated base and motion stage feedforward controllers, where

$$\boldsymbol{V}_{FF,i}(s) = \underbrace{-k_{f,i}^{-1}\begin{bmatrix}\boldsymbol{D}_f L_i & \boldsymbol{K}_f L_i + \boldsymbol{D}_f R_i & \boldsymbol{K}_f R_i & \boldsymbol{a}_3 & \boldsymbol{a}_2 & \boldsymbol{a}_1 & \boldsymbol{a}_0\end{bmatrix}}_{W} \cdot \underbrace{\begin{bmatrix}\boldsymbol{a}_f & H_n\boldsymbol{a}_f & H_n^2\boldsymbol{a}_f & rs^3 & rs^2 & rs & r\end{bmatrix}^T}_{\tilde{\psi}} \tag{3.38}$$

$$I_{FF,m}(s) = \underbrace{m_{eq}\begin{bmatrix}1 & \frac{d_m}{m_m} & \frac{k_m}{m_m}\end{bmatrix}}_{\boldsymbol{W}} \cdot \underbrace{\begin{bmatrix}rs^2 & rs & r\end{bmatrix}^T}_{\tilde{\boldsymbol{\psi}}} \tag{3.39}$$

To explain this in a more general sense, $\boldsymbol{V}_{FF,i}(s)$ and $I_{FF,m}(s)$ are denoted by the controller output signal $u_{FF}(k)$, where k is the iteration number. Then $u_{FF}(k)$ is rewritten to align the notation with the algorithm.

$$u_{FF}(k) = \underbrace{\begin{bmatrix}\tilde{\psi}^T(k) & \dots & 0\\ \vdots & \ddots & \vdots\\ 0 & \dots & \tilde{\psi}^T(k)\end{bmatrix}}_{\tilde{\Psi}(k)} \underbrace{\begin{bmatrix}(W_{(1,:)}(k))^T\\ \vdots\\ (W_{(n,:)}(k))^T\end{bmatrix}}_{w(k)} \tag{3.40}$$

where n is the nth row in W. As such, $w(k)$ is a vertical concatenation of the transposed rows of W and $\tilde{\Psi}(k)$ is a blockdiagonal repetition of $\tilde{\psi}^T(k)$. Now the goal of the algorithm is to minimize the error as a result of a mismatch between estimated and 'true' parameters. This process can be described as

$$e(k) = P_2(\Psi(k)w(k) + \hat{\Psi}(k)\hat{w}(k|k-1)) \tag{3.41}$$

where

$$\hat{\Psi} = \Psi + \tilde{\Psi} \tag{3.42}$$

$$\hat{w} = w + \tilde{w}. \tag{3.43}$$

Here, $\hat{\Psi}$ is the regressor that may be corrupted with noise. For the isolated base, $\hat{\Psi}$ is partly constructed from the measurement of $\boldsymbol{a}_f$ and therefore contains noise. For the motion stage, $\hat{\Psi}$ is constructed solely from the reference signal which is analytically determined and does not contain noise. $\hat{w}$ is the parameter vector that contains an estimation error.
The error of the process which is minimized is $e(k)$. For the isolated base the error is the measurement of the isolated base acceleration

$$\hat{\boldsymbol{e}}_i(k) = \boldsymbol{a}_i(k) + \boldsymbol{n}_i(k). \tag{3.44}$$

where $\hat{\boldsymbol{e}}_i(k)$, $\boldsymbol{a}_i(k)$ and $\boldsymbol{n}_i(k) \in \mathbb{R}^{6\times 1}$. For the motion stage the error is the difference between the reference and the measured local motion stage position.

$$\hat{e}_m(k) = r(k) - \Delta x_m(k) + n_m(k) \tag{3.45}$$

In both cases, n is the measurement noise. For the isolated base this is considered uncorrelated to the measurement noise of the floor acceleration that is part of $\hat{\Psi}$. The error is filtered by the estimated inverse of P_2 to align the error with the feedforward output. A noise shaping filter N is added to attenuate high frequency noise and make $N\hat{P}_2^{-1}$ causal. Thus, the filtered error is obtained by

$$\hat{e}_{filt}(k) = N(q)\hat{P}_2^{-1}(q)\hat{e}(k). \tag{3.46}$$

Then following a Kalman scheme [20], the rest of the algorithm will go as follows.
The covariance matrix of the innovation is given by

$$S(k) = N(q)\hat{\Psi}(k)P(k|k-1)\hat{\Psi}^T(k)N^T(q) + R. \tag{3.47}$$

Then the Kalman gain can be calculated as

$$K(k) = N(q)\hat{\Psi}(k)P(k|k-1)S^{-1}(k). \tag{3.48}$$

The parameter and covariance update law yield

$$\hat{w}(k|k) = \hat{w}(k|k-1) + K(k)\hat{e}_{filt}(k) \tag{3.49}$$

$$P(k|k) = P(k|k-1) - K(k)N(q)\hat{\Psi}(k)P(k|k-1) \tag{3.50}$$

respectively, where $\hat{w}(k|k)$ is the updated estimate of the true system parameters $w(k)$. For the next iteration the parameters are considered equal to the updated parameters with some unknown error.

$$\hat{w}(k+1|k) = \hat{w}(k|k) + \tilde{w}(k) \tag{3.51}$$

$$P(k+1|k) = P(k|k) + Q \tag{3.52}$$

R and Q are the covariance matrices of the measurement noise and process noise respectively. R represents the uncertainty in the measurement model, usually due to sensor noise. As such, if R is relatively high with respect to P, the measurement will not affect the parameters a lot and vise versa. Q represents the uncertainty in the prediction model, which in this case can be interpreted as the variation in parameters over time. Electric parameters like resistance are affected by temperature. As such, the armature resistance of the VCM's is likely to change over time due to the power dissipation as a result of this same resistance. Therefore, parameters that include armature resistance may have more uncertainty than pure mechanical parameters such as damping and stiffness that are not likely to change much over time. Looking at 3.38, the armature resistance is quite abundant within the parameter vector of the isolated base. Additionally, Q will serve as a lower limit when P becomes very small as a result of convergence. This allows the parameter adaptation to continue after convergence, similar to a forgetting factor applied in RLS algorithms [12].
The initial covariance is a measure of the uncertainty of the initial parameters. It greatly determines the initial adaptation rate. If all parameters are properly identified, the initial covariance will be relatively small. However, if identification is poor then parameter uncertainty will be high and the initial covariance will be relatively large. Here, care must be taken as a high initial uncertainty along with a low measurement uncertain may result in an adaptation rate that is too fast and cause instability.
For the isolated base the algorithm in its current form is computationally expensive as $\hat{\boldsymbol{\Psi}} \in \mathbb{R}^{6\times 132}$ and $\boldsymbol{P} \in \mathbb{R}^{132\times 132}$. Due to the blockdiagonal nature of $\hat{\boldsymbol{\Psi}}$, the covariance matrix $\boldsymbol{P}$ is blockdiagonal as well. Therefore, each row in equation 3.40 can be calculated individually as

$$u_{FF,n}(k) = \underbrace{\left[\tilde{\psi}^T(k)\right]}_{\tilde{\Psi}(k)} \underbrace{\left[(W_{(n,:)}(k))^T\right]}_{w(k)} \tag{3.53}$$

where each row is denoted by n. Note that the regressor vector $\tilde{\psi}^T(k)$ has to be calculated only once for all rows. As a result S, the covariance matrix of the innovation, reduces to a scalar, avoiding matrix inversion. This greatly improves calculation efficiency. The motion stage is a SISO system so S is already a scalar.

Figure 3.7 shows the control scheme of figure 3.1 updated with the proposed parameter adapatation.

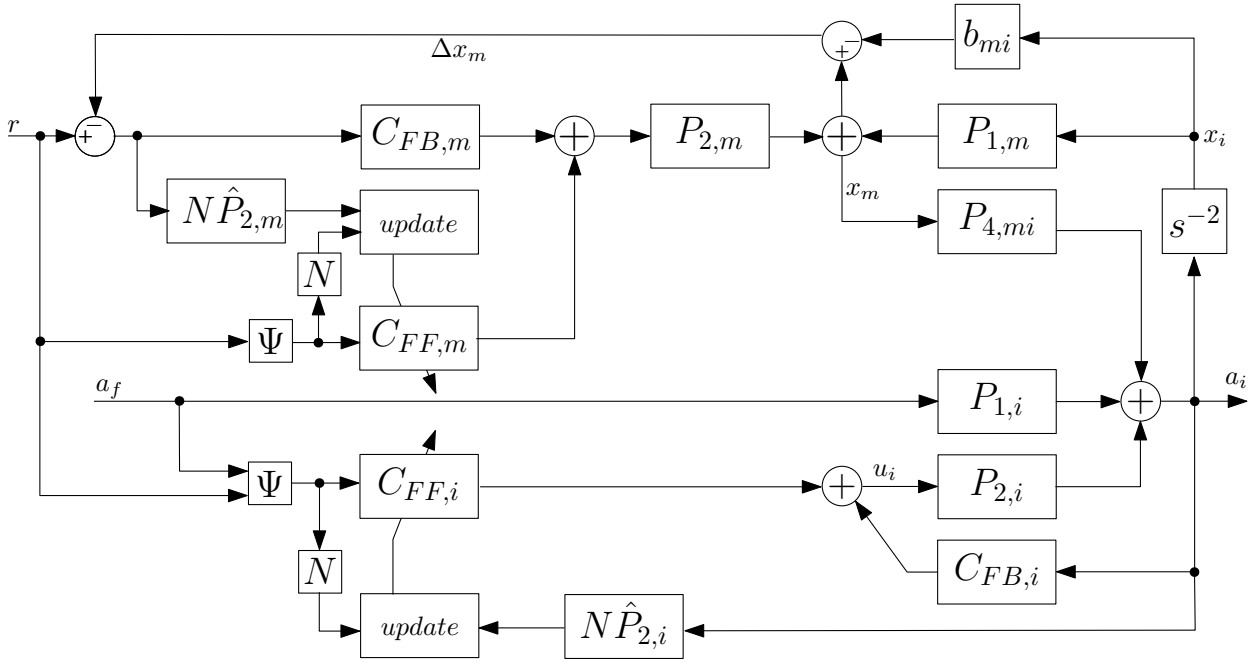

Figure 3.7: Control scheme AVIS with adaptation

Note that it is actually the filtered error that is minimized and not necessarily the error itself. The cost function is defined as the expectation of the (filtered) error squared, commonly known as the mean squared error.

$$\epsilon = E(\hat{e}^2_{filt}(k)) \tag{3.54}$$

It is important to realize that the algorithm will always attempt to convergence to a set of parameters that minimizes the error for the system in its current state.

Simulation

A simulation model based on the scheme from the previous chapter is build using Simscape Multibody. The proposed controller is implemented and tested. The simulation setup and results are presented in this chapter.

4.1 Simulation setup

The model as described in Chapter 2 is build using Matlab/Simulink and the Simscape Multibody library. This allows for easy testing of control algorithms in preparation for practical implementations. The visual editor also provides great flexibility for testing with different system configurations or parameters.
An argument against usage of an external library is that the underlying physics is not transparent and may give rise to inaccuracies. This library does have a proven trackrecord [21] such that the risk is assumed minimal. Additionally, the use of model-based feedforward control provides an implicit sanity check of the simulation model with the equations of motion derived earlier. An overview of the model layout is given in figure 4.1.

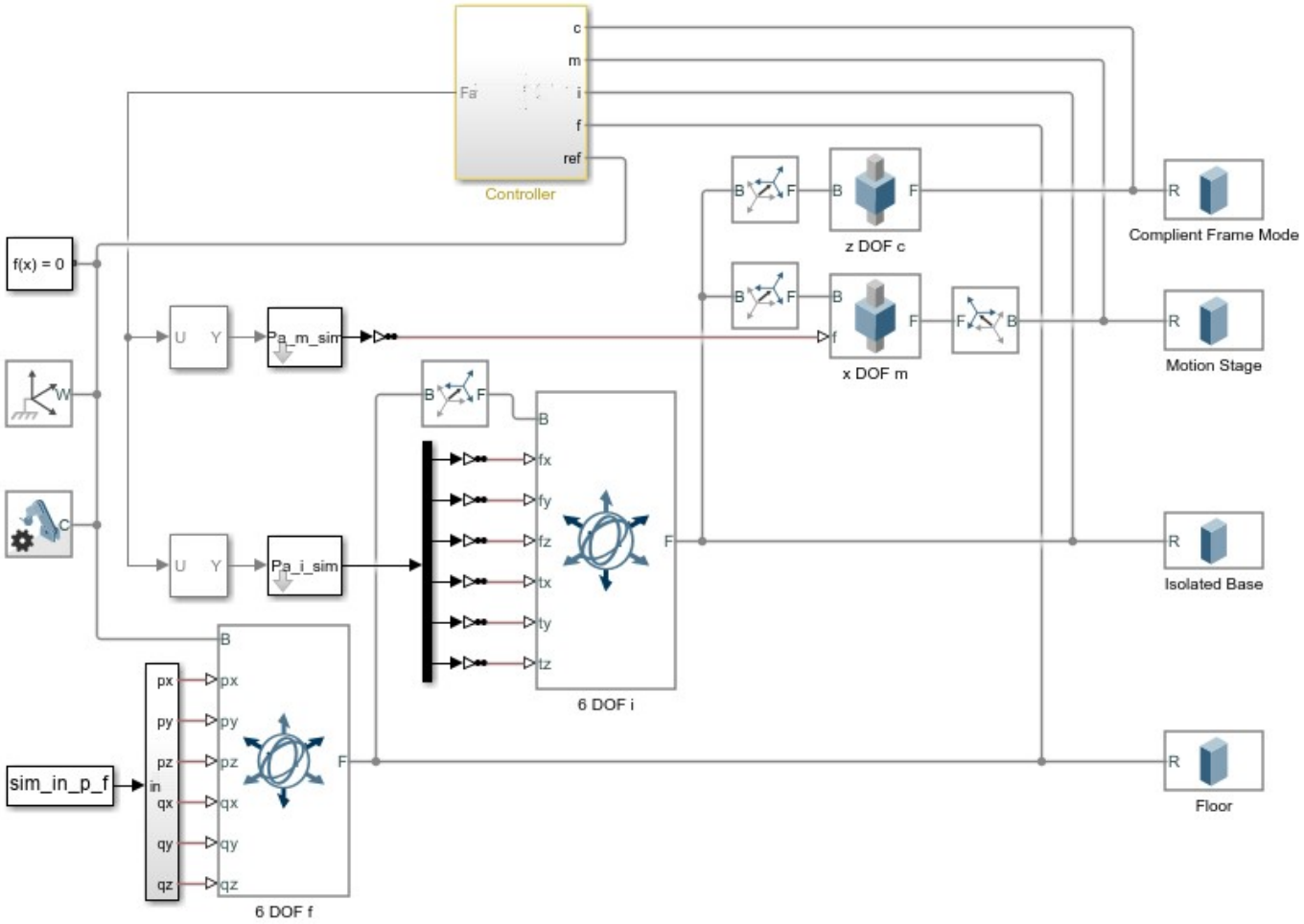

Figure 4.1: Simulation setup

Similar to the model described, four bodies can be distinguished, being the floor, the isolated base, the motion stage and the compliant frame mode. Joints are provided stiffness and damping properties such that

their presence is not immediately visible. The floor is connected to a reference frame by means of a 6-DOF 'bushing' joint. The displacement and its derivates a provided as input. Therefore, its mass and inertia are properties and not of interest for the calculation. The isolated base is connected to the floor by means of a similar joint, however in this case the displacement is a result of forces and torques acting on the body. The motion stage and compliant frame mode are connected to the isolated base by means of a 1-DOF 'prismatic' joint. In addition, a rigid transformation is used to enforce a constraint in x and z direction respectively, local to the coordinate frame of the isolated base. The controller obtains the floor accelerations, isolated base accelerations and motion stage displacement and interfaces with the actuators. The actuators are connected to the joints of the isolated base and motion stage where the force is applied to the system.

The simulations are conducted with a controller sample rate of 9 kHz. Initial parameter estimates where derived from [3], [5], [22] and later corrected with identification results.
Since the floor is considered rheonomic, its position is a disturbance input to the model. The power of the input noise is based on the ASML floor spectrum [23]. The reference path of the motion stage is a third degree displacement function, shown in figure 4.2. The derivates are determined analytically according to [19, sec. 14.3].

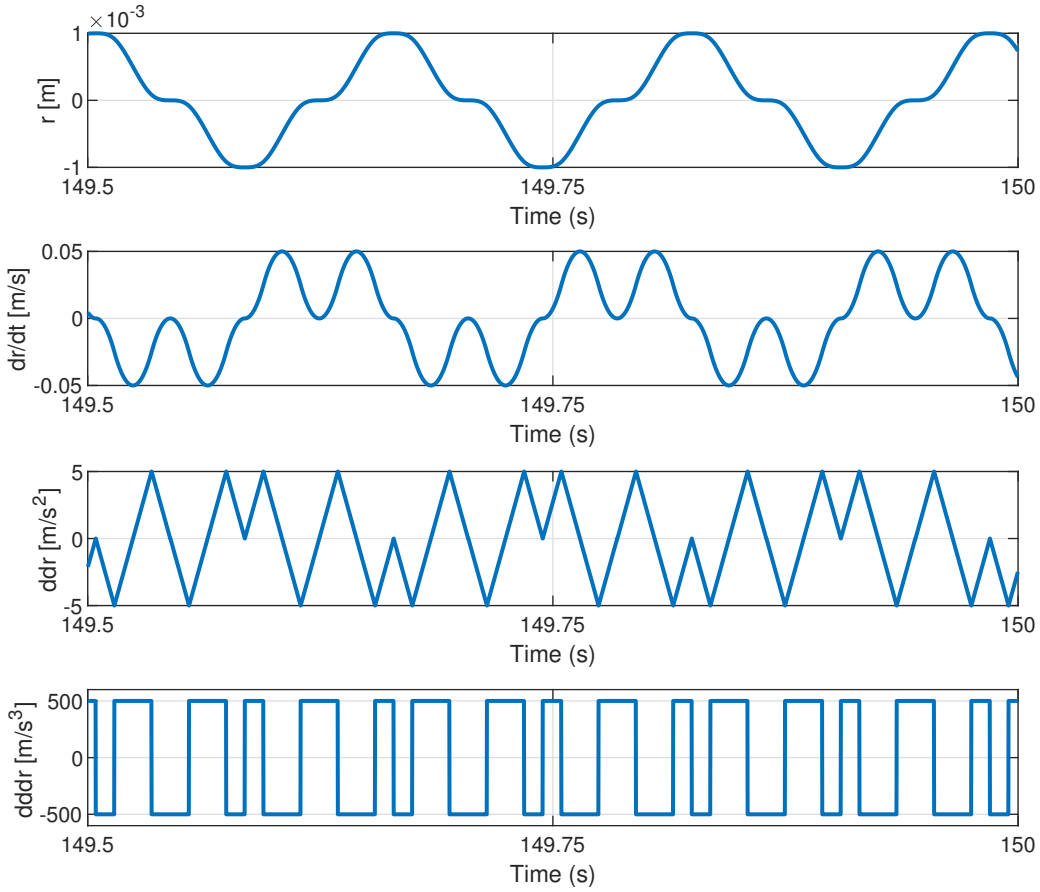

Figure 4.2: Motion stage reference position, velocity, acceleration and jerk in the time domain.

Figure 4.3 shows a PSD of the motion stage reference and its derivates. As the jerk is a square wave, the frequency spectrum typically contains the odd harmonics. Then in the frequency domain the acceleration (n=1), velocity(n=2) and displacement(n=3) are obtained by multiplication with $\frac{1}{s^n}$. The signals do not contain a lot of power outside the base frequency and the odd harmonics such that below the base frequency the PSD becomes inaccurate.

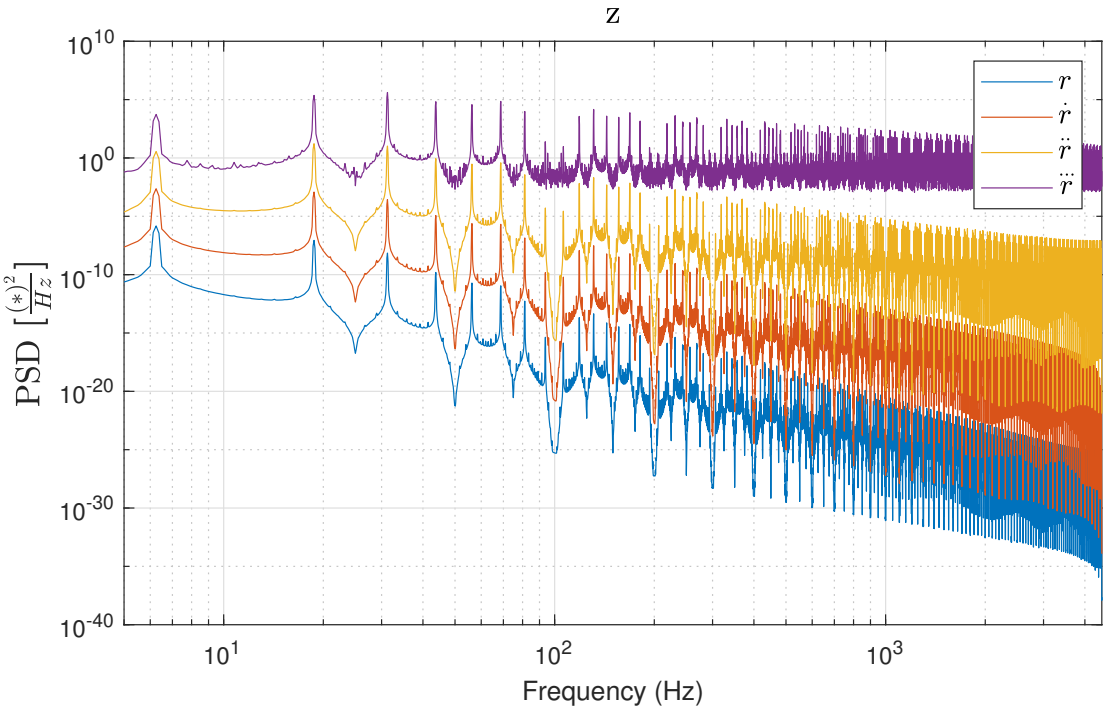

Figure 4.3: PSD of the motion stage reference.

Based on the results of [12], [22], 3rd order weak integrators with a cutoff frequency of 1 Hz are used. The pass band of the noise shaping filter is set from 5 to 500 Hz.

4.2 Simulation results

Figure 5.6 shows the power spectral density of the isolated base acceleration for a passive system, feedback control and feedback + feedforward control. The feedback controller of the isolate base greatly dampens the first resonance peak for all axes. With feedback and feedforward control an additional reduction is achieved between 1 and 500 Hz, whereas the greatest performance gain is achieved between approximately 5 and 300 Hz.

The effect of the motion stage is predominantly visible for the x and θ_y directions, which is to be expected as its only degree of freedom is in the x-direction local to the isolated base. The frequencies at which the peaks occur coincide with PSD of the reference signal provided in figure 4.3. With only feedback control the 3rd and 5th harmonic are somewhat dampened compared to the passive system. For other harmonics the effect is very limited. With feedback and feedforward control the disturbance at fundamental frequency of the motion stage is completely cancelled for the x-axis. Higher harmonics persist but are greatly reduced. As for the y-axis the trend is roughly the same, however the fundamental frequency is not completely cancelled.

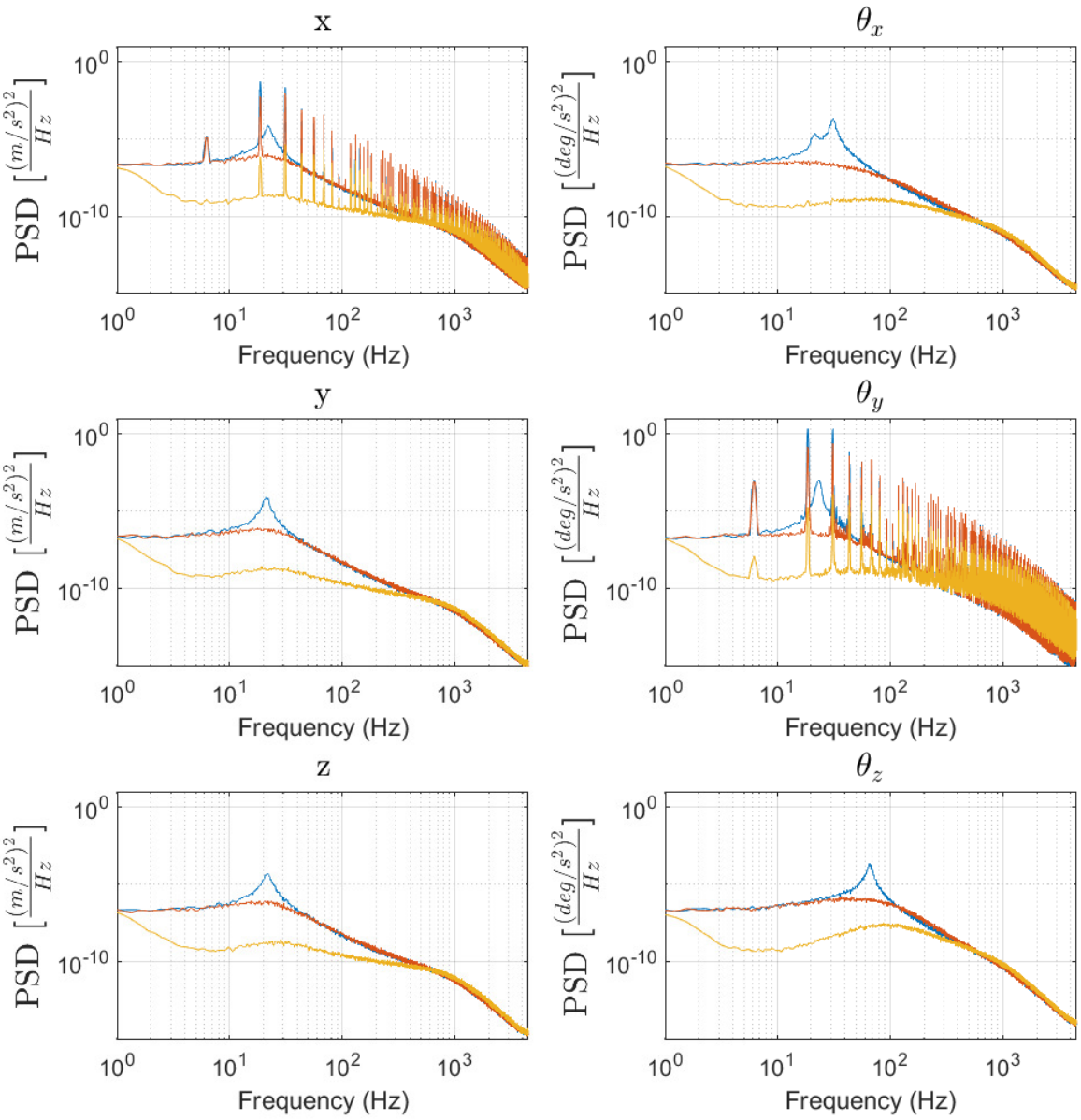

Figure 4.4: Power spectral density of a_i for a passive system (blue), feedback control (red) and feedback + feedforward control (yellow).

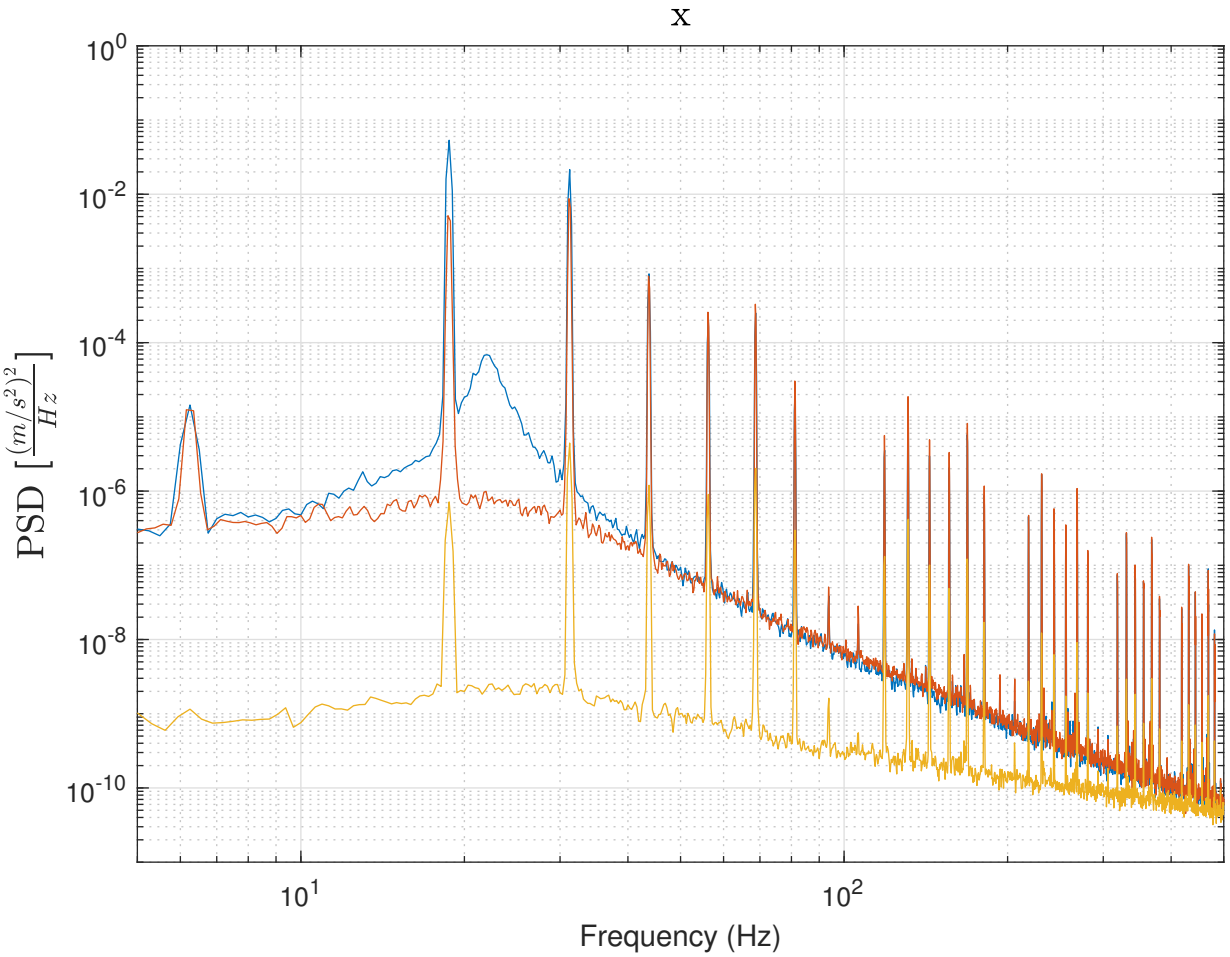

Figure 4.5: Power spectral density zoom of $a_{i,x}$ for a passive system (blue), feedback control (red) and feedback + feedforward control (yellow).

	1	3	5	7	9	11	13
Passive	1.45e-5	5.34e-2	2.15e-2	8.45e-4	2.17e-4	2.51e-4	2.15e-5
FB	1.23e-5	4.73e-3	7.61e-3	6.54e-4	2.04e-4	2.49e-4	2.22e-5
FB + FF	1.15e-9	7.15e-7	4.44e-6	1.20e-6	9.02e-7	2.02e-6	2.96e-7

Table 4.1: PSD values for $a_{i,x}$ at odd harmonics of the motion stage reference. The fundamental frequency, or 1st harmonic, is 6.25 Hz.

Figure 4.5 shows the PSD of the isolated base acceleration for the x-axis where the frequency range of 5 to 500 Hz is highlighted. Up to the resonance frequency, the power density for feedback + feedforward control is at least two orders of magnitude lower than for passive and feedback control. Also, the improved attenuation of motion stage harmonics for feedback + feedforward control continues up to at least 500 Hz. In table 4.1 the values of the power spectral densities at the odd harmonics of the motion stage are listed up until the 13th harmonic, which is at 81.25 Hz.

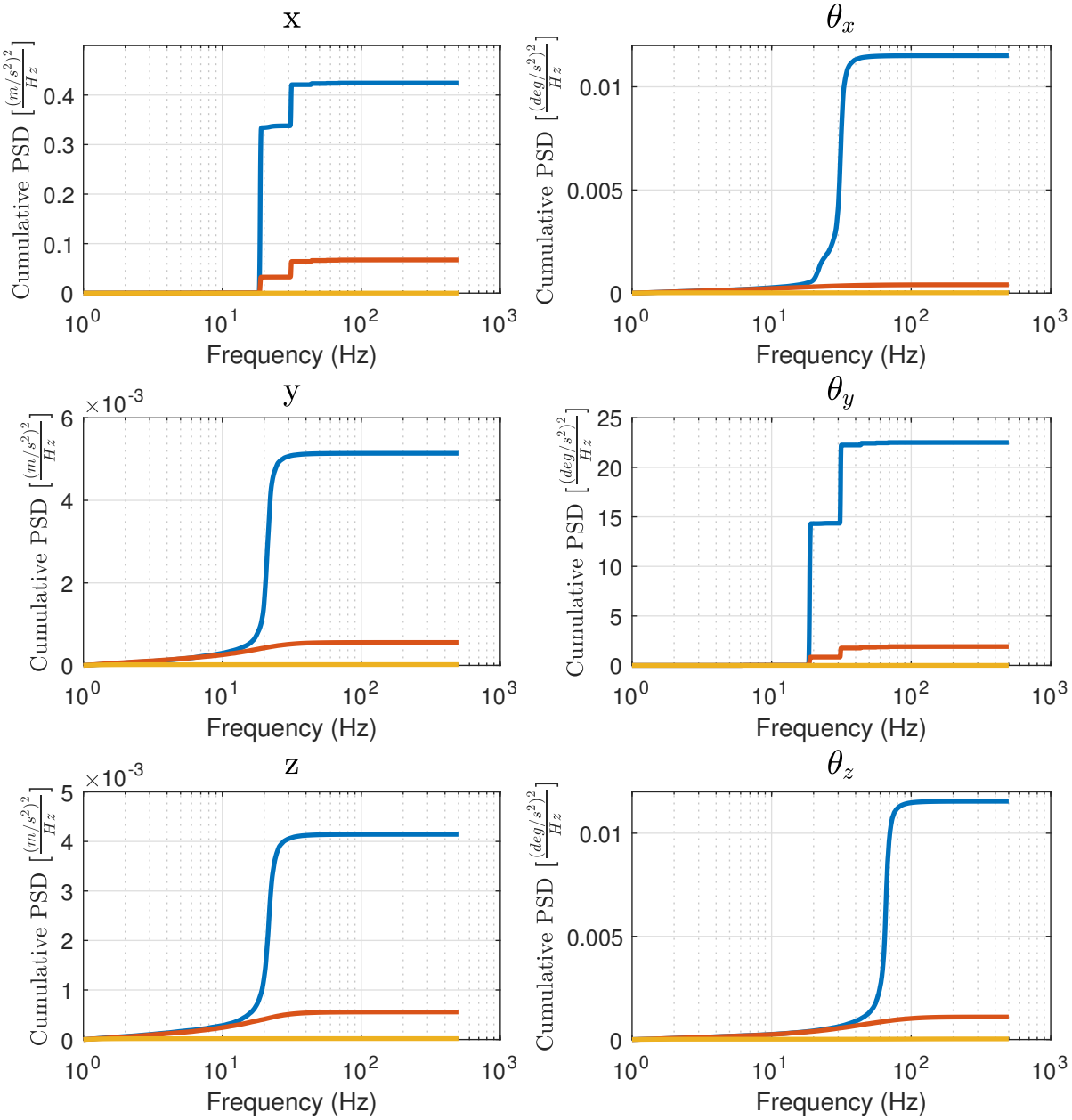

Figure 4.6: Cumulative power spectral density of $a_{i,x}$ for a passive system (blue), feedback control (red) and feedback + feedforward control (yellow).

Figure 4.6 shows the cumulative sum of the power spectral densities shown in figure 4.4 up to 500 Hz. The plot line of feedback + feedforward controlled system is more or less similar to the baseline in any graph, indicating the significant performance gain that is achieved.

4.3 Adaptation

To test the adaptation algorithm, system parameters are initialized at 10% of their expected optimal value. Figure 4.7 shows the evolution of the estimated motion stage parameters over time. The estimated mass and stiffness appear nearly perfect, the damping is slightly off. The convergence time here is typically around 10 seconds. As the motion stage is considered a relatively simple SISO system, it provides a nice validation of the filtered error Kalman approach.

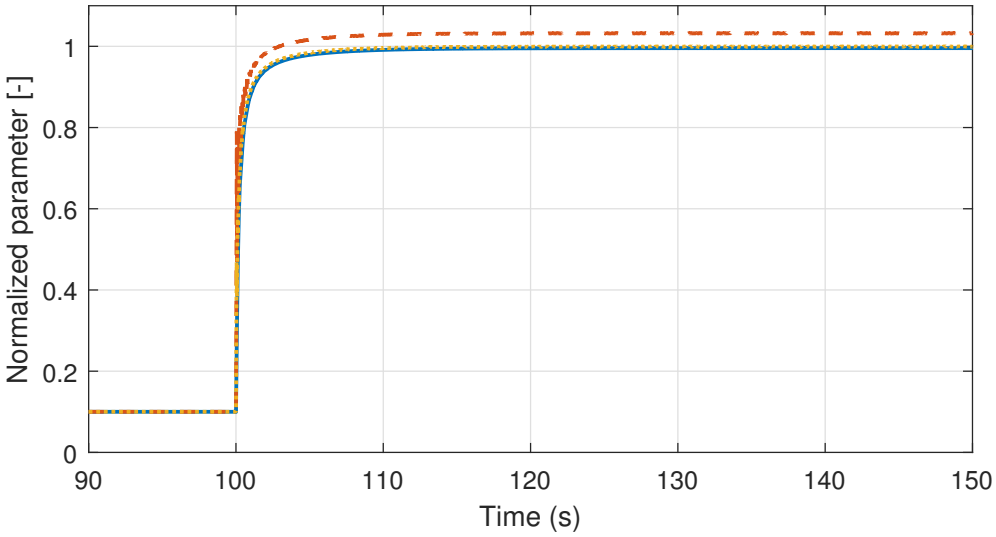

Figure 4.7: Evolution of normalized motion stage parameters over time. The adaptation starts at t = 100 s. Nominal parameter values are m = 0.1689 kg, d = 3.6671 Ns/m, k = 614.4 N/m.

Figure 4.8 shows the evolution of the motion stage error over time for different combinations of isolated base controllers. The motion stage controller is always a mixed feedback/feedforward controller with adaptation. For the passive system the maximum error is around 2.65 μm. With only feedback enabled this reduces to 1.3 μm. Additional feedforward pushes error down further to maximum of 600 nm and with adaption the best result is obtained with a maximum error of approximately 400 nm.
The motion stage error after isolated base controller adaptation is highlighted in the right figure of 4.8, along with the motion stage reference signal. There appears to be some repetitive pattern still present in the error, suggesting that more performance gain is possible.

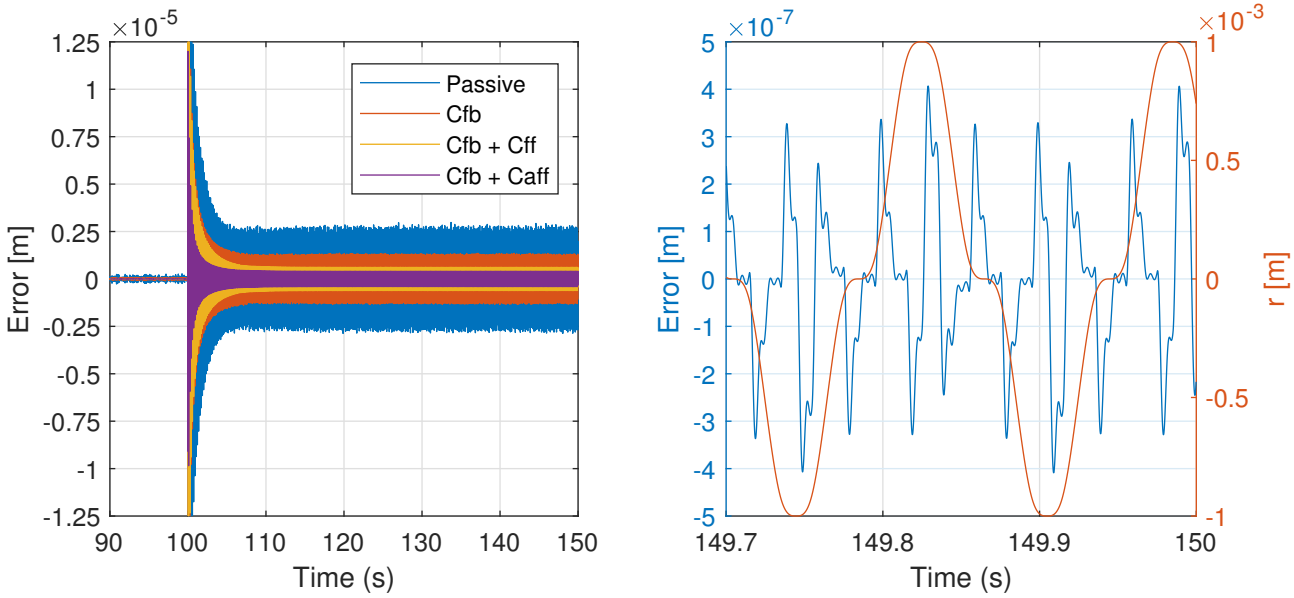

Figure 4.8: Evolution of the motion stage error over time for different controllers (left) and a zoom on the error after adaptation (right). The adaptive feedforward controller is denoted as C_{aff}.

Figures 4.9 and 4.10 show the power spectral density filtered error and unfiltered error of the isolated base respectively. Note that the error here is the measured isolated base acceleration. Although the goal is to minimize the actual unfiltered error, the filtered error is that what is actually being minimized. As such, within the pass band of the noise shaping filter, minimization of the filtered error should also lead to minimization of the unfiltered error. The passband of the noise shaping filter is 5 to 500 Hz. According to figures 4.9 and 4.10 this is also the range where for most axes the performance gain with adaptation is achieved. The effect of the high pass characteristic of the noise shaping filter is clearly visible below 5 Hz, where the PSD of the filtered error decreases. The low pass characteristic beyond 500 Hz in combination with the natural low pass characteristics of the system results in a very steep rolloff.
The isolated base acceleration in figure 4.10 shows some performance gain with respect to floor induced

disturbance attenuation, as is best illustrated by axes θ_x and θ_z, where the motion stage has little effect. The same effect is visible on the x and θ_y axes, however not on the y and z axes. After adaption the PSD of the x direction shows some improvement with respect to the base frequency of the motion stage reference. For the θ_y direction no real improvement is shown for this frequency. Both directions show large improvements with respect to higher harmonics up to approximately 100 Hz.

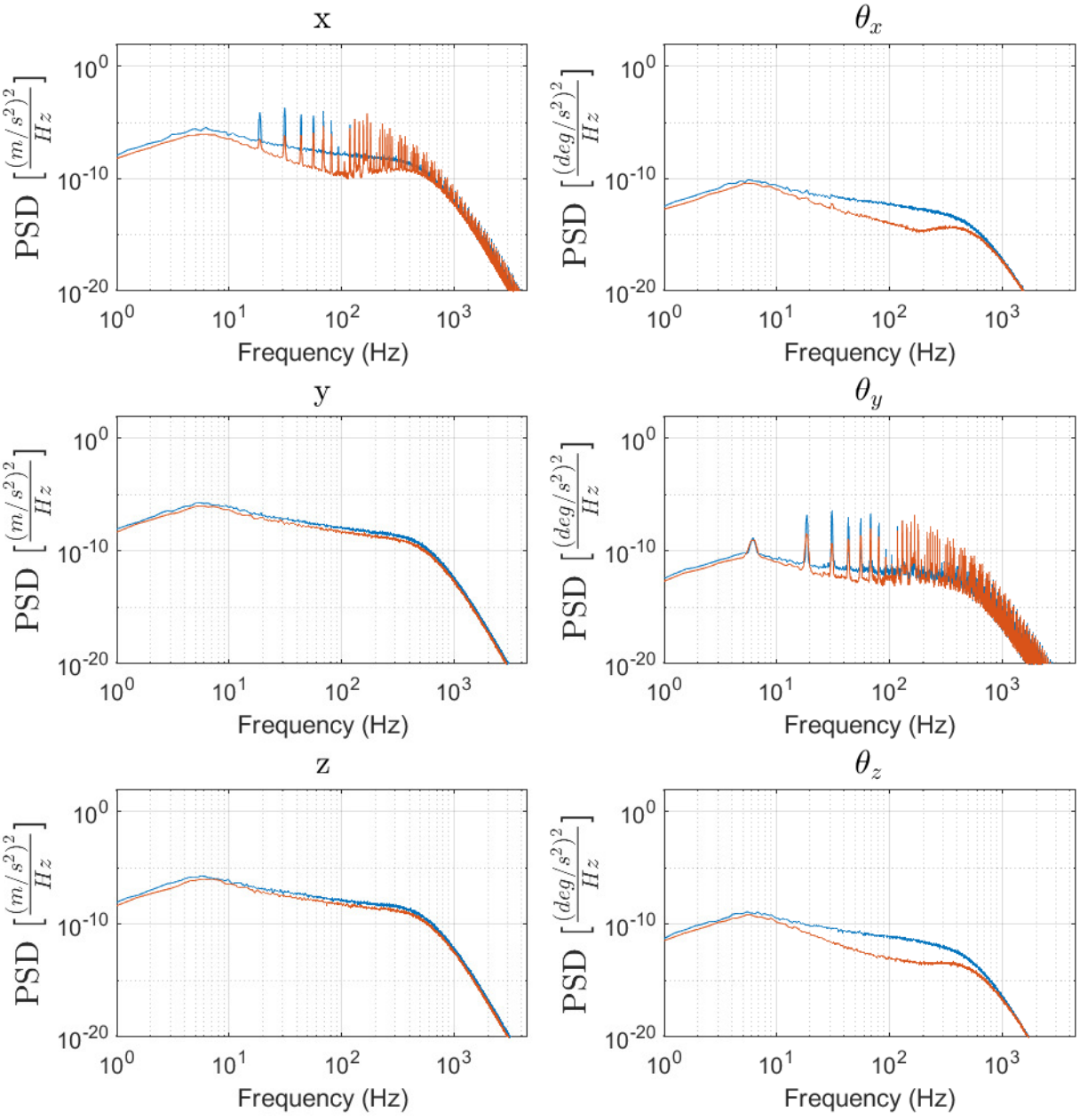

Figure 4.9: Filtered error of the isolated base before (blue) and after (red) adaptation

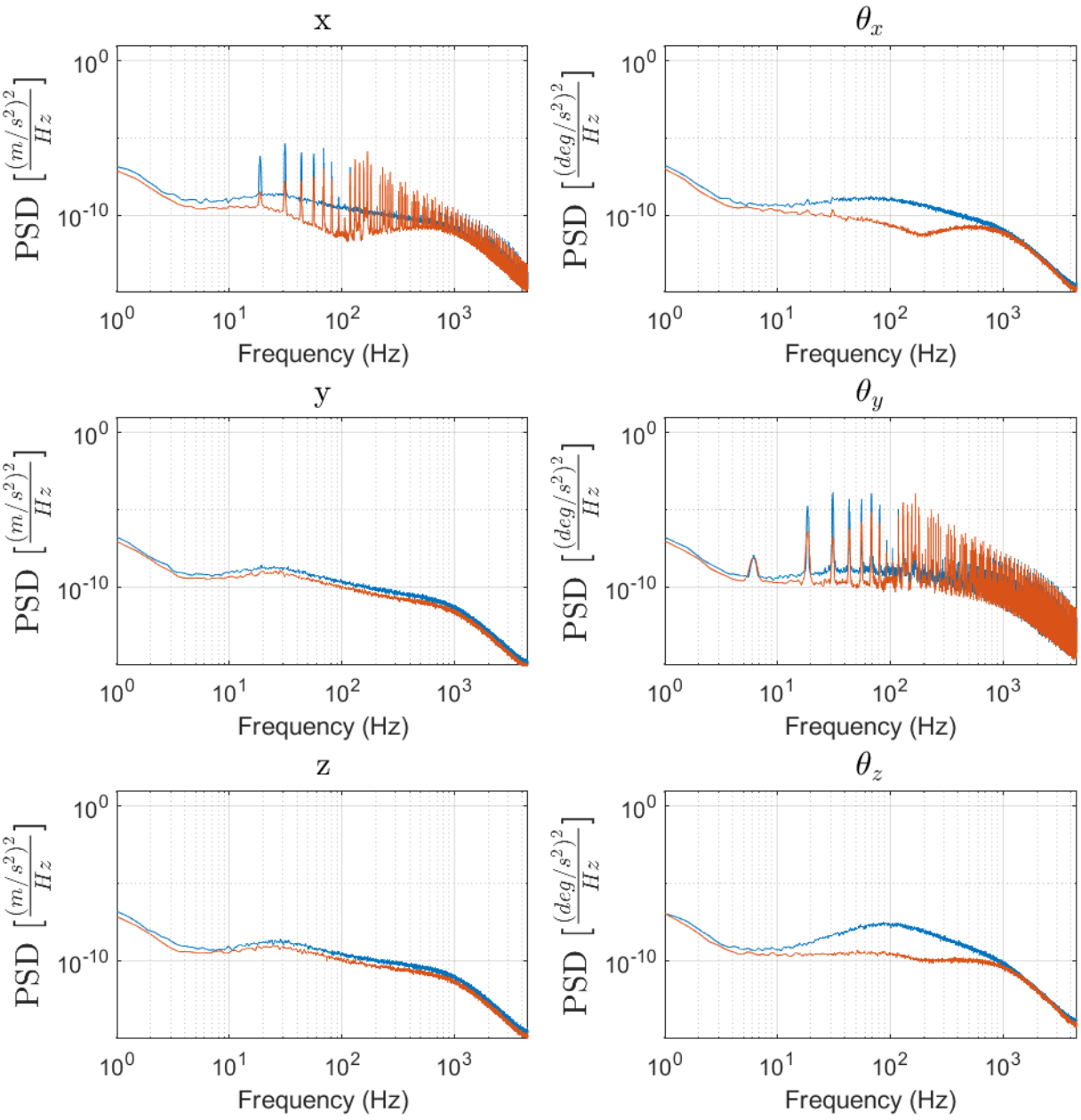

Figure 4.10: Unfiltered error of the isolated base before (blue) and after (red) adaptation

Experimental Validation

The proposed controller is implemented and tested on an experimental setup. The secondary paths of the isolated base and motion stage are identified and the results are presented in this chapter.

In order to validate several aspects of the simulation model, the experimental AVIS setup as depicted in figure 5.1 is used.

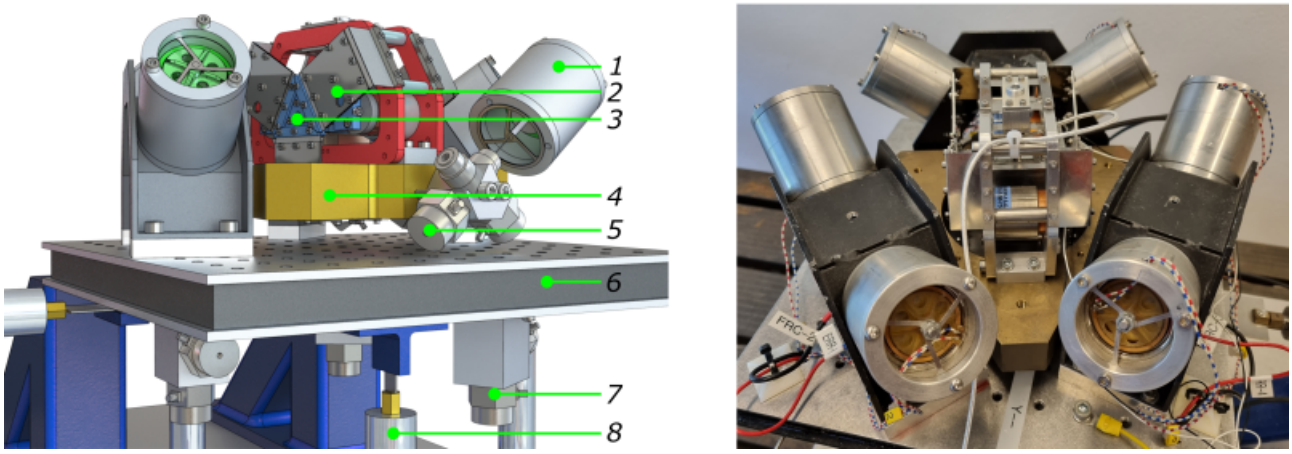

Figure 5.1: CAD render[8] (left) and photo (right) of the experimental AVIS with VCM's (1), flexure based straight guide (2), motion stage (3), isolated base (4), isolated base accelerometers (5), floor (6), floor accelerometers (7), piezoelectric actuators (8). In the CAD render some parts a left out for better visualization.

A total of six 'legs' can be distinguished that suspend the isolated base to the floor. Each leg consists of a VCM in series with a wire flexure. The VCM coil is connected to the housing by means of a flexure based membrane. The wire flexure is connected to this coil on one end and to the isolated base on the other. Its stiffness is most dominant in axial direction, which is highly desired, as other directions (e.g. bending or torsional) will introduce parasitic stiffness [4]. The positions of the legs is chosen such that six DOF can be constrained, resulting in an exact-constraint platform. On top the isolated base, the motion stage is mounted. It consists of a shuttle that is suspended to a rigid frame by means of six folded leaf springs. Two VCM's lateral to the shuttle provide the motion. Finally, there is the compliant frame mode, which is suspended to the same rigid frame by means of leaf springs. It is not actuated and therefore a passive component. The floor is excited with three piezoelectric actuators, allowing for excitation along the axes z, θ_x and θ_y.
The setup is equipped with a total of twelve accelerometers, six for the floor and six for the isolated base. The isolated base accelerometers are located in line with each wire flexure, defining the local frame for each leg. The controller is implemented on a dSpace MicroLabBox at a sample rate of 9 kHz. The accelerometer interface is provided by Nexus 2692-0S4 (B&K) amplifiers. The VCM's for actuation of the isolated base are of type VM4032-250 (Geeplus), whereas the motion stage VCM's are of type AVM30-15 (Akribis). TA-105 amplifiers (Trust) provide the actuator interface for the VCM's, where the isolated base VCM's are voltage controlled and the motion stage VCM's current controlled. The motion stage position is measured using a Ti4000 (Renishaw) encoder.

5.1 System identification

The error filter defined in equation 3.46 contains an estimate of P2. Proper identification of P2 is required, as its accuracy is important in the adaptation process. The general structure is defined in equation 3.24. Figure

5.2 shows the FRF of P2 in the local frame for each 'leg'. Parasitic modes start to become prominent after approximately 500 Hz.

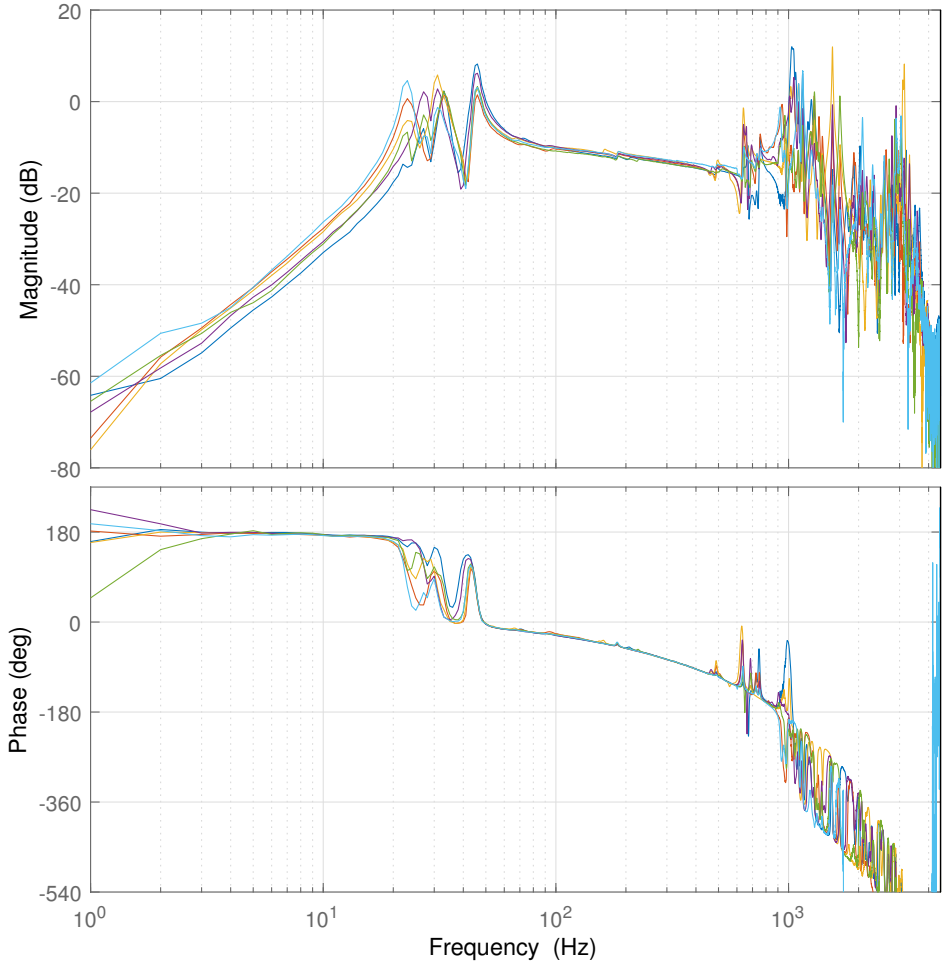

Figure 5.2: Local FRF of P2.

Using the structure from 3.24, transfer functions s^2G and $P_{a,i}$ can be distinguished. With the assumption that the actuator dynamics are relatively accurate by using datasheet parameters, s^2G is fitted with such that the total transfer function matches the FRF. Two delay samples are added for DAC and ADC conversion. This is depicted in figure 5.3. The first natural frequency is at approximately 35 Hz.

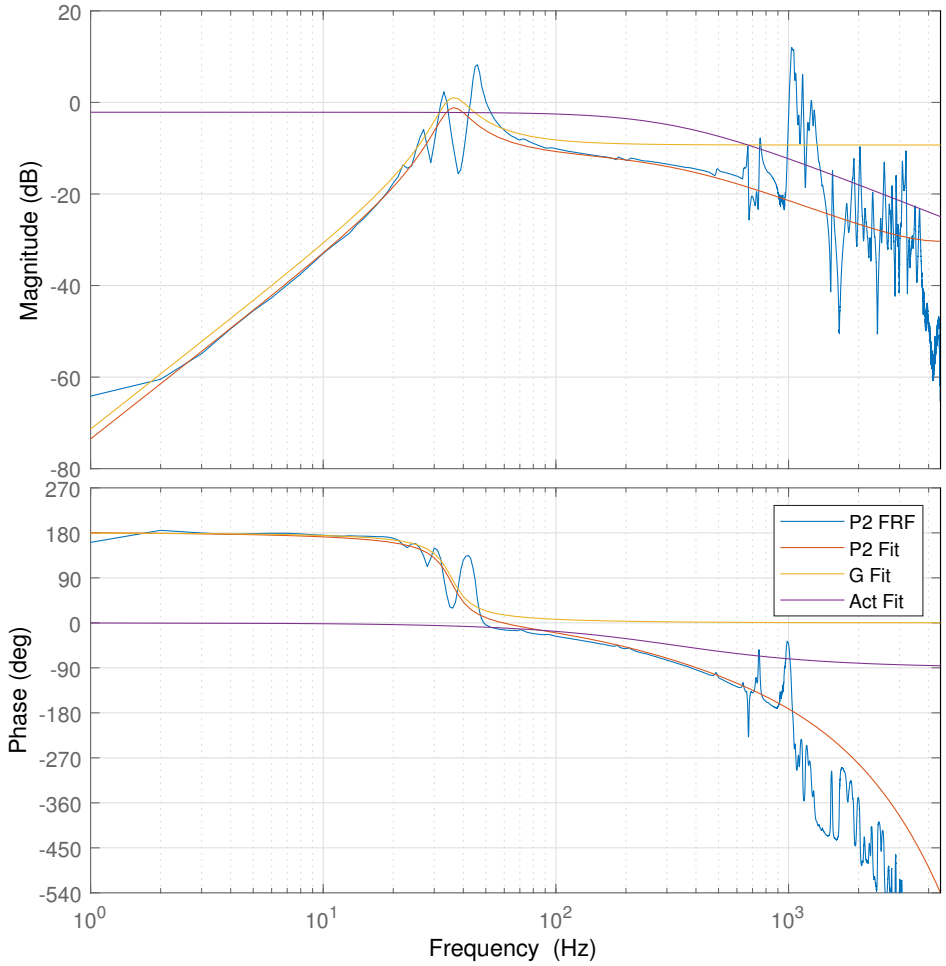

Figure 5.3: FRF and fit of $P_{2,i}$

The motion stage FRF along with a parametric fit is provided in figure 5.4. The fit is based on the structure provided in equation 3.20. This structure is reasonably accurate up to 400 Hz, where parasitic modes start to become visible. The first natural frequency is at approximately 9.6 Hz. Beyond the first natural frequency the transfer function is predominantly described by $\frac{1}{m_{eq}s^2}$, thus this can be used to determine m_{eq}. Then the relative damping can be approximated from the FRF. Two samples time delay were added to match the phase. This can be explained by DAC and ADC in the loop.

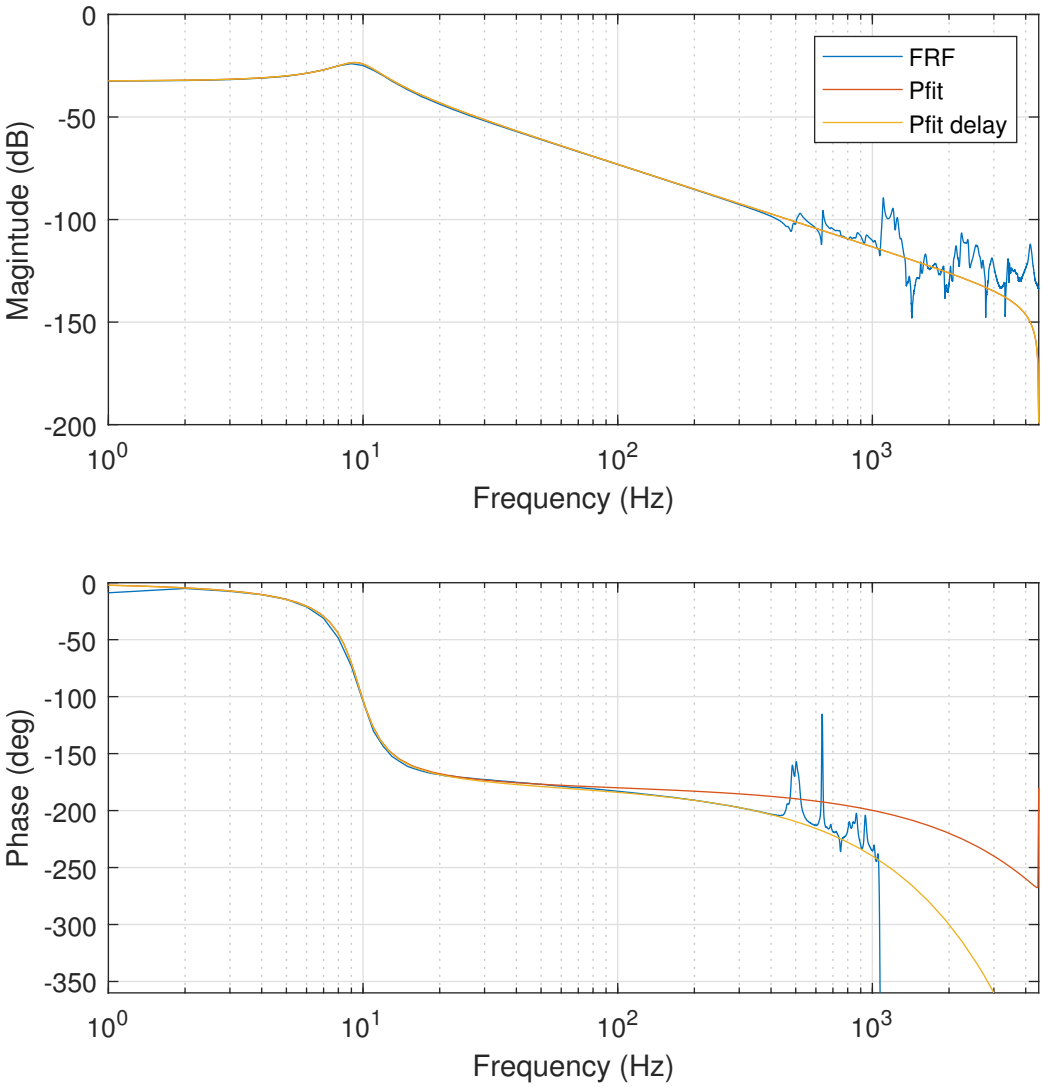

Figure 5.4: FRF and fit of $P_{2,m}$

5.2 Results

Figure 5.5 shows the filtered error of the isolated base. Although most prominent for the x and θ_y directions, the fundamental frequency of the motion stage is clearly visible in all directions, suggesting a coupling between the axes. It appears that some parasitic modes start to emerge around 200 Hz.

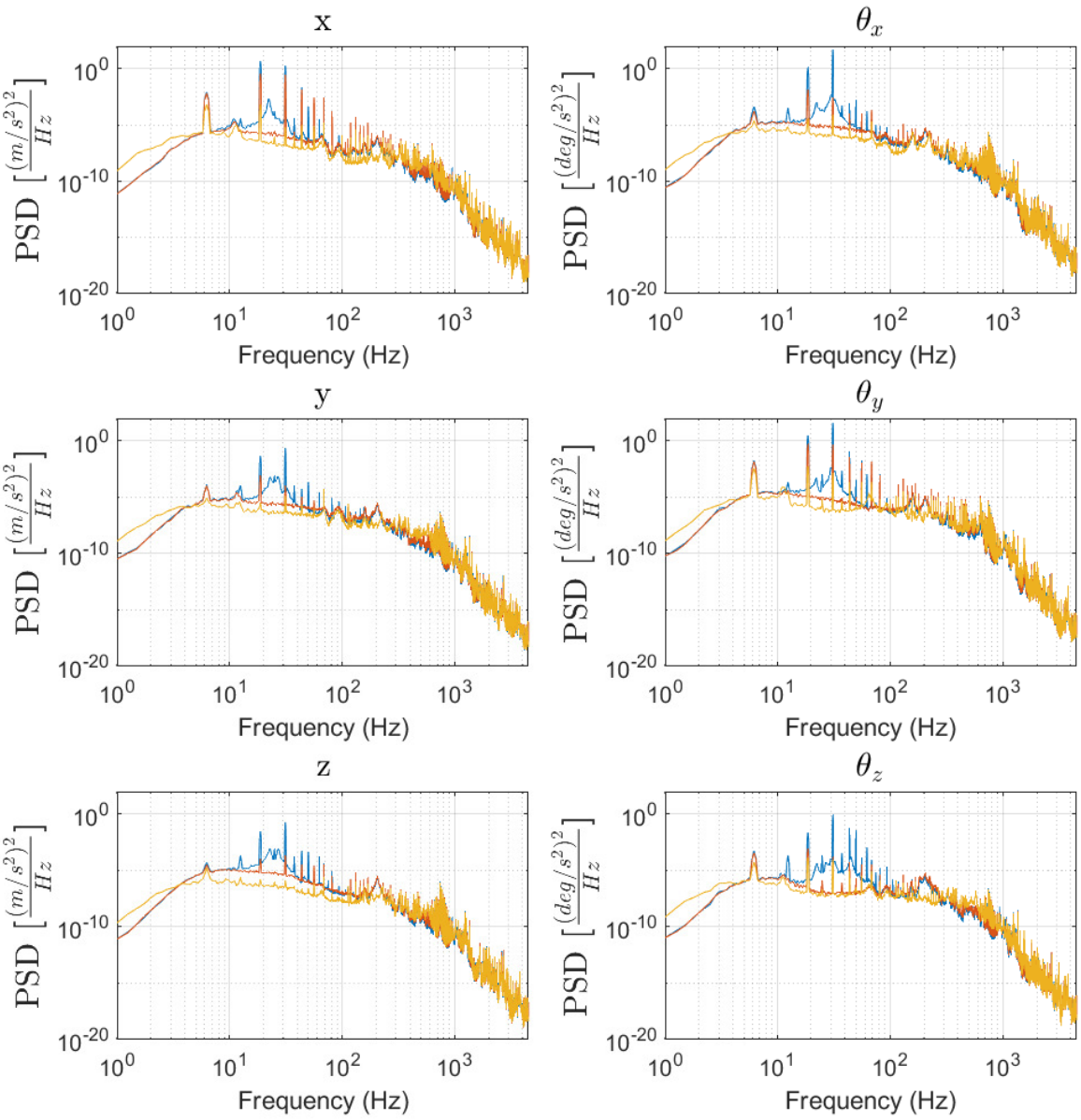

Figure 5.5: Power spectral density of the filtered error for a passive system (blue), feedback control (red) and feedback + feedforward control (yellow).

Figure 5.6 shows the acceleration of the isolated base. The results resemble those of the filtered error.

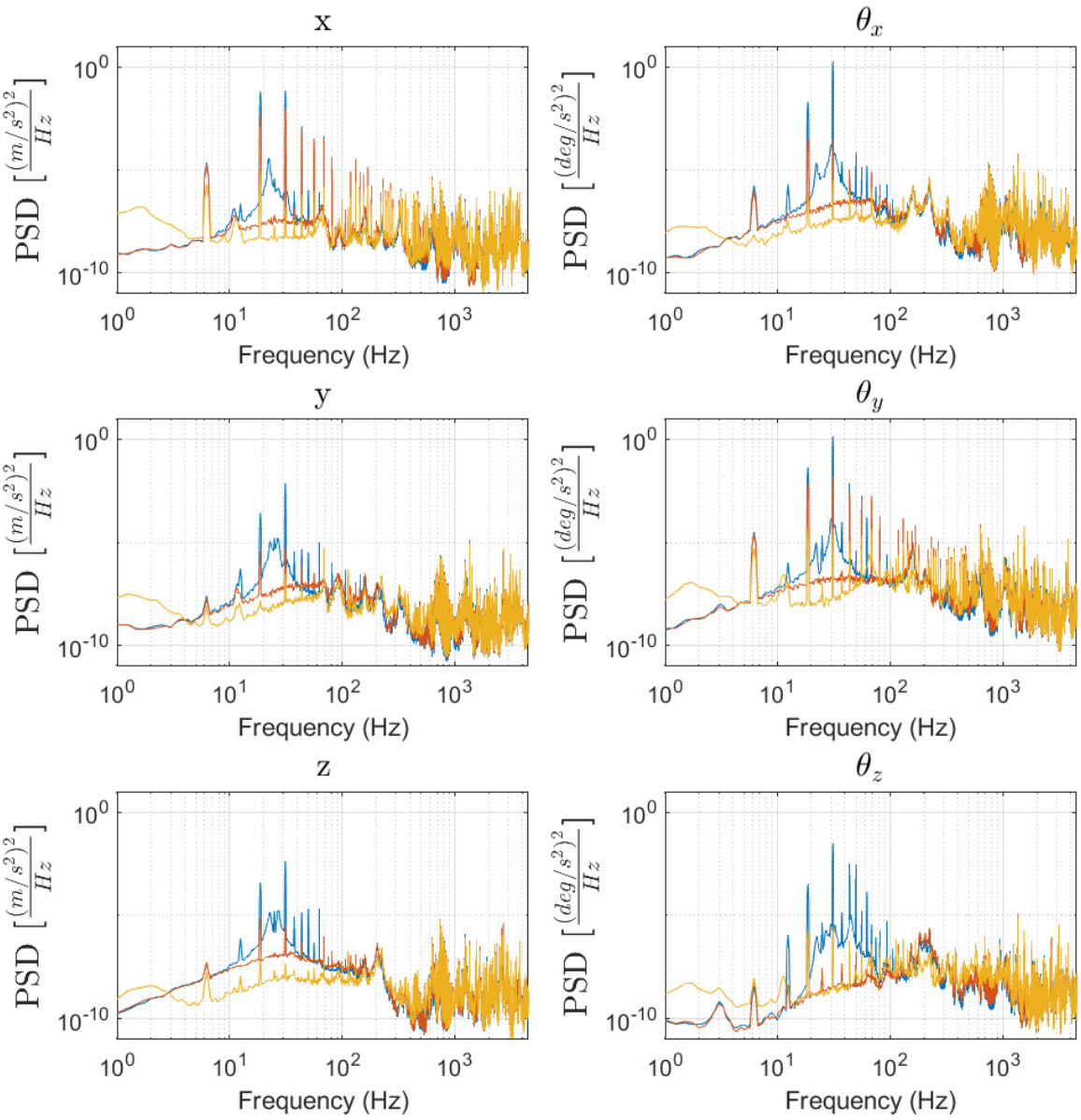

Figure 5.6: Power spectral density of a_i for a passive system (blue), feedback control (red) and feedback + feedforward control (yellow).

The feedback + feedforward controller appears to provide a substantial performance gain up to approximately 100 Hz for all axes except θ_z.

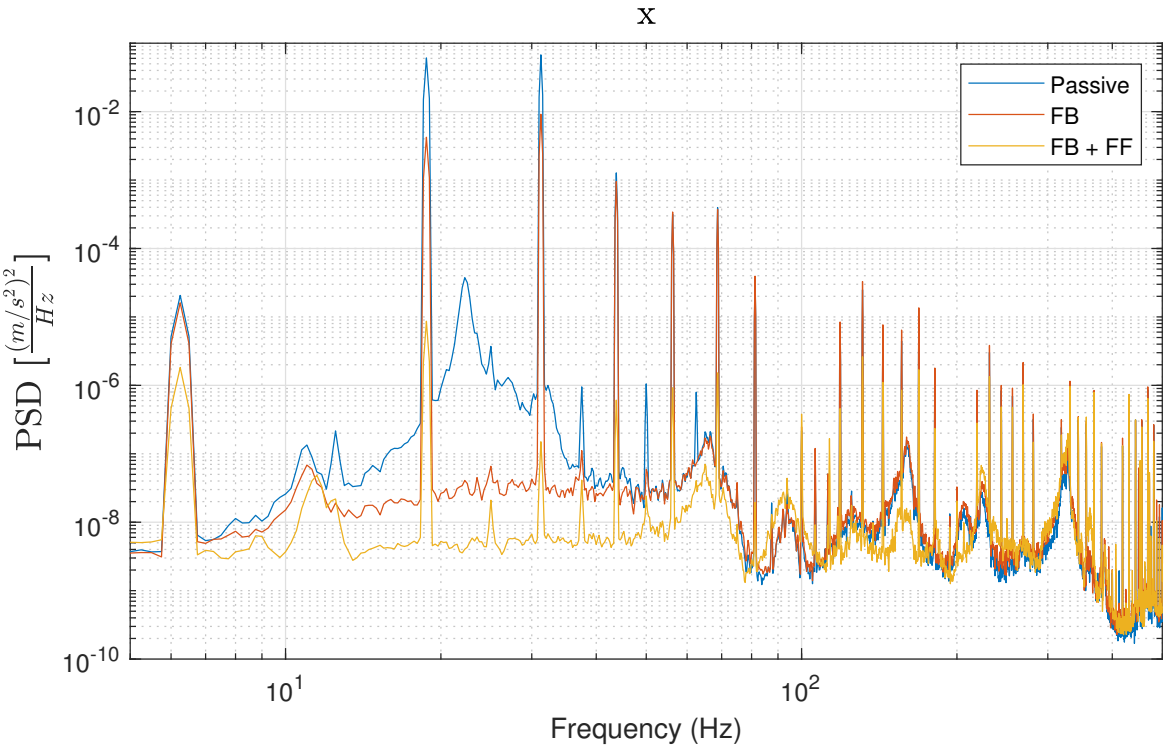

Figure 5.7: Power spectral density zoom of $a_{i,x}$ for a passive system (blue), feedback control (red) and feedback + feedforward control (yellow).

	1	3	5	7	9	11	13
Passive	2.06e-5	6.04e-2	6.66e-2	1.25e-3	3.09e-4	3.85e-4	3.37e-5
FB	1.60e-5	4.19e-3	9.04e-3	9.34e-4	3.33e-4	3.62e-4	3.80e-5
FB + FF	1.82e-6	8.58e-6	1.48e-7	5.97e-7	8.97e-7	1.48e-6	1.90e-8

Table 5.1: PSD values for the $a_{i,x}$ at odd harmonics of the motion stage reference. The fundamental frequency, or 1st harmonic, is 6.25 Hz.

Figure 5.7 shows the PSD of the isolated base acceleration for the x-axis where the frequency range of 5 to 500 Hz is highlighted. Feedback + feedforward control clearly provides a performance improvement up to approximately 200 Hz with respect to the passive system and feedback control. Especially for the odd motion stage harmonics. The peak around 10 Hz is most likely the resonance frequency of the motion stage. In table 5.1 the values of the power spectral densities at the odd harmonics of the motion stage are listed up until the 13th harmonic, which is at 81.25 Hz.

Conclusion & Discussion

In this thesis, a method is proposed to systematically determine the equations of motion for an active vibration isolation system with motion stage and compliant frame mode. The equations of motion have been used to construct the feedforward controllers in an adopted mixed feedback/feedforward control scheme. A filtered-error Kalman adaption is proposed in order to cope with unknown or time-varying system parameters. These propositions have been incorporated in a simulation model and validated on an experimental AVIS setup.

6.1 System dynamics and control strategy

A method is proposed to systematically determine the equations of motion for an active vibration isolation system with motion stage and compliant frame mode. By extending the generalized coordinate vector with local variables, the construction of the equations of motion was greatly simplified. These equations are then used to determine the actuator forces required to cancel disturbances acting on the sensitive payload. Using these forces, a feedforward controller is constructed that is linear in the parameters. A filterd-error Kalman adaptation is proposed to update the parameters and account for parameter uncertainty and time-varying parameters.

6.2 Simulation

Using a Simulink Simscape model, the proposed controller was implemented and tested. It is shown that a mixed feedback/feedforward controller greatly mitigates vibrations for all axes and their rotations within the passband of the noise shaping filter. Due to its orientation, the effect of the motion stage disturbance is predominantly visible on the x and θ_y axes. For the x-axis the effect of the motion stage at its fundamental frequency appears almost completely attenuated. As for the θ_y-axis there is still some residual disturbance at this frequency. For both axes the harmonics are still present, however strongly reduced compared to the passive system or solely feedback control. With the mixed feedback/feedforward approach the maximum motion stage error improved from 2.65 μm to 600 nm. Applying parameter adaptation resulted another reduction to a maximum error of around 400 nm. The adaptation improved overall disturbance attenuation for all axes within the passband of the noise shaping filter. The harmonics of the motion stage showed a strong reduction. For the $theta_y$ axis the fundamental frequency did not appear to be affected after adaption.

6.3 Experimental validation

The designed controller was implemented and experimentally validated on an existing AVIS. An efficient implementation of the filter-error Kalman algorithm allowed for a realtime sample rate of 9 kHz. Overall, the mixed feedback/feedforward controller showed improved disturbance attenuation on all axes, with respect to the passive system. Also, the harmonics of the motion stage that were visible on all axes due to coupling, were clearly reduced. The maximum motion stage error reduced from 3 μm with the passive system to approximately 300 nm after adaptation of the feedforward parameters.

6.4 Discussion

It is important to consider the context that has lead to the aforementioned findings such that it may serve as a starting point for further research. Therefore, some important elements of this thesis will be discussed here.

The proposed method for deriving the equations of motion works nicely because the system is kinematically solvable and all relevant independent coordinates are available as measurements. The motion stage, that represents some critical process, is a relatively simple system with a single DOF that may

approximate a wide variety of systems with a single dominant mode. The applied method, however, remains applicable for more complex motion stages, as long as the system is kinematically solvable. For example, the motion stage could have three DOF's as long as they are all available for measurement. If the system is not kinematically solvable, then some states must be estimated. Since there is already an adaptive law that uses these states to update the parameters, it turns into a combined parameter and state estimation problem, which increases the complexity quite drastically.

The equations of motion for this system are nonlinear and quite extensive. In order to obtain the linear feedforward equations, the position of the isolated base was set to zero, leaving only forces that do not directly depend on the isolated base position. Conveniently this leaves out any crossterms between isolated base coordinates and other coordinates, such that the result is a controller that is linear in the parameters. The downside is that this is a great simplification and the performance of the feedforward controller decreases when the position of the isolated base is not zero, for example due to parameter mismatch, unmodelled disturbances or delays. This is likely one of the reasons that there are still residuals of the motion stage disturbance visible in the PSD's of the isolated base acceleration. Since the complete generalized coordinate vector and its derivatives are readily available in the simulation model, it is suggested to use these to calculate the original nonlinear equations of motion. This may identify some principal components that are missing in the current controller as a result of the simplification.
A possible improvement could be to linearize the system around its estimated position and then apply the adaptation. This is presumably computationally more expensive, such that it may introduce a tradeoff with the sample rate.

Through the update law a feedback loop is constructed within the disturbance feedforward controller. This loop can also be found in figure 3.7. The effect of this loop on stability is not considered, but could be a topic for further research.

Although a common trend was observed between the PSD's for the isolated base of the simulation and experimental setup, they are definitely not the same. To some extent this can be explained by the fact that the number piezoelectric actuators available to excite the floor was limited to three, excitation of the floor was only possible in z, θ_x and θ_y direction. It is therefore not possible to provide all floor axes with equal noise power density. It is likely that this also affects parameter adaptation as some parts of the spectrum may have more 'weight' in the adaptation process. The latter does not necessarily explain any differences between PSD's, but is important to consider when comparing parameter convergence.
The model used for simulation did not have coupling between the axes and also no parasitic modes. The experimental results clearly indicate their presence. Although they do not necessarily have to be included in the model, it is important to consider these phenomena when exploring stability and robustness of the controlled system.
Another point of interest is that a (Gaussian) noise model for the sensors was implicitly assumed by use of the filtered-error Kalman adaptation, but actual sensor dynamics were not included in the simulation model. In any case, it is important to either include them in the model or verify experimentally that they can be neglected.
The floor is considered rheonomic. In practice, however, this is not the case. The isolated base actuators exert reaction forces on the floor, causing vibrations that backpropagate through the suspension. This creates another transfer path that will likely affect parameter adaptation as these vibrations correlate with the applied actuator forces to some extent. To include this path, the model could be extended with finite floor stiffness as described for a 1-DOF system in [5, Ch. 4].

Bibliography

[1] C. Collette, S. Janssens, K. Artoos, and C. Hauviller, "Active vibration isolation of high precision machines," *Diamond Light Source Proceedings*, vol. 1, no. MEDSI-6, e1, 2010. DOI: 10.1017/S2044820110000134.

[2] A. Preumont, "Vibration control of active structures: An introduction," in Apr. 1999, vol. 96. DOI: 10.1023/A:1004398914135.

[3] M. Beijen, "Disturbance feedforward control for vibration isolation systems: Analysis, design, and implementation," English, Ph.D. dissertation, Eindhoven University of Technology, 2018, ISBN: 978-90-386-4459-2.

[4] D. Tjepkema, "Active hard mount vibration isolation for precision equipment," Ph.D. dissertation, Nov. 2012. DOI: 10.3990/1.9789036534185.

[5] T. van der Poel, "An exploration of active hard mount vibration isolation for precision equipment," Ph.D. dissertation, May 2010. DOI: 10.3990/1.9789036530163.

[6] W.-H. Chen, J. Yang, L. Guo, and S. Li, "Disturbance-observer-based control and related methods—an overview," *IEEE Transactions on Industrial Electronics*, vol. 63, no. 2, pp. 1083–1095, 2016. DOI: 10.1109/TIE.2015.2478397.

[7] P. Fraanje, "Robust and fast schemes in broadband active noise and vibration control," English, Ph.D. dissertation, Netherlands, 2004, ISBN: 9789090180021.

[8] S. Spanjer, R. Kelder, and W. Hakvoort, "Active vibration isolation with integrated virtual balance mass for a motion stage," English, in *euspen's 22nd International Conference and Exhibition, Geneva, CH, May/June 2022*, R. Leach, A. Akrofi-Ayesu, C. Nisbet, and D. Phillips, Eds., EUSPEN, 2022, pp. 195–198.

[9] M. Beijen, M. Heertjes, J. Van Dijk, and W. Hakvoort, "Self-tuning mimo disturbance feedforward control for active hard-mounted vibration isolators," *Control Engineering Practice*, vol. 72, pp. 90–103, 2018, ISSN: 0967-0661. DOI: https://doi.org/10.1016/j.conengprac.2017.11.008. [Online]. Available: https://www.sciencedirect.com/science/article/pii/S0967066117302666.

[10] M. Beijen, J. van Dijk, W. Hakvoort, and M. Heertjes, "Self-tuning feedforward control for active vibration isolation of precision machines," *IFAC Proceedings Volumes*, vol. 47, no. 3, pp. 5611–5616, 2014, 19th IFAC World Congress, ISSN: 1474-6670. DOI: https://doi.org/10.3182/20140824-6-ZA-1003.01208. [Online]. Available: https://www.sciencedirect.com/science/article/pii/S1474667016424882.

[11] M. Beijen, M. Heertjes, R. Voorhoeve, and T. Oomen, "Evaluating performance of multivariable vibration isolators: A frequency domain identification approach applied to an industrial avis," in *2017 American Control Conference (ACC)*, 2017, pp. 3512–3517. DOI: 10.23919/ACC.2017.7963490.

[12] W. Hakvoort and M. Beijen, "Filtered-error rls for self-tuning disturbance feedforward control with application to a multi-axis vibration isolator," English, *Mechatronics*, vol. 89, 2023, ISSN: 0957-4158. DOI: 10.1016/j.mechatronics.2022.102934.

[13] R. Munnig Schmidt, G. Schitter, and J. van Eijk, *The design of high performance mechatronics. High-tech functionality by multidisciplinary system integration.* English. Netherlands: IOS Press, 2011, ISBN: 978-1-60750-825-0. DOI: http://dx.doi.org.10.3233/978-1-60750-826-7-i.

[14] B. Stenlund and F. Gustafsson, "Avoiding windup in recursive parameter estimation," *Preprints of Reglermöte 2002*, pp. 148–153, Jan. 2002.

[15] J. Schilder, *Reader dynamics 3 - flexible multibody dynamics*, University of Twente, 2015.

[16] X. Wang, Z. Jiao, and S. Wu, "Design and study of digital power driver controller for a kind of voice coil motor," in *IEEE 10th International Conference on Industrial Informatics*, 2012, pp. 596–601. DOI: 10.1109/INDIN.2012.6301181.

[17] M. Boerlage, M. Steinbuch, P. Lambrechts, and M. van de Wal, "Model-based feedforward for motion systems," in *Proceedings of 2003 IEEE Conference on Control Applications, 2003. CCA 2003.*, vol. 2, 2003, 1158–1163 vol.2. DOI: 10.1109/CCA.2003.1223174.

[18] P. Lambrechts, M. Boerlage, and M. Steinbuch, "Trajectory planning and feedforward design for electromechanical motion systems," *Control Engineering Practice*, vol. 13, no. 2, pp. 145–157, 2005, ISSN: 0967-0661. DOI: https://doi.org/10.1016/j.conengprac.2004.02.010. [Online]. Available: https://www.sciencedirect.com/science/article/pii/S0967066104000462.

[19] R. Aarts, G. Romer, H. Koroglu, J. van Dijk, and C. van Keulen, *Design and control of mechatronic systems*, University of Twente, 2021.

[20] F. van der Heijden, R. Duin, D. de Ridder, and D. Tax, *Classification, parameter estimation and state estimation: an engineering approach using matlab*, English. United States: Wiley, Sep. 2004, ISBN: 978-0-470-09013-8. DOI: 10.1002/0470090154.

[21] P. Noskievič and D. Walica, "Design and realisation of the simulation model of the stewart platform using the matlab-simulink and the simscape multibody library," in *2020 21th International Carpathian Control Conference (ICCC)*, 2020, pp. 1–5. DOI: 10.1109/ICCC49264.2020.9257249.

[22] R. Kelder, "Active vibration isolation with an active stage," English, M.S. thesis, University of Twente, 2021.

[23] S. Spanjer and W. Hakvoort, "Optimal active vibration isolation system design using constrained h2 control," in *IFAC Mechatronics*, 2020.